

THE FLORIDA STATE UNIVERSITY
FAMU-FSU COLLEGE OF ENGINEERING

COMPARATIVE ANALYSIS OF THE POWER OUTPUT OF CRYSTALLINE
PHOTOVOLTAIC (PV) MODULES USING SOLAR TRACKING SYSTEM

By

THOMAS P. ANTHONY

A Thesis submitted to the
Department of Industrial Engineering
in partial fulfillment of the
requirements for the degree of
Master of Science

Degree Awarded:
Fall Semester, 2006

The members of the Committee approve the thesis of Thomas P. Anthony defended on the 15th of October, 2006.

Yaw A. Owusu
Professor Directing Thesis

James Simpson
Committee Member

Carl A. Moore
Committee Member

Approved:

Chuck Zhang, Interim Chair, Industrial Engineering

Chen Jen Chen, Dean, College of Engineering

The Office of Graduate Studies has verified and approved the above named committee members.

This work is dedicated to my parents Alexandrine and George Anthony

“I can do all things through Christ who strengthens me.”

Philippians 4:13

ACKNOWLEDGEMENTS

I would like to acknowledge the Florida A&M University Center for Cutting Edge Technologies, directed by Dr. Yaw A. Owusu, for its support throughout the thesis process. I would also like to thank the United States Department of Education in Washington, D.C through the Title I Program for the financial support of the Research Center for Cutting Edge Technologies (RECCET).

Special thanks go to the staff of the Research Center for Cutting Edge Technologies (RECCET), especially the directorate: Dr. Yaw A. Owusu my major professor, Mr. Ronald T. Cutwright, Dr. Tarsha Dargan and Dr. Hans Chapman. Many thanks go to the other two members of my thesis committee, Dr. Carl Moore and Dr. James Simpson for technical support and thesis guidance respectively.

It would be remiss of me not to thank dear relatives, friends and colleagues who sacrificed their time to assist me at one point or another. Most notable are: Mrs. Margaret M. Thomas, B.A. Hon, Ms. Yoshino N. Woodard, MSIE, Mr. Jonnattan T. Ugarte, BSME, Ms. Charney A. Davy, MSME, and Ms. Sihle Wilson.

Not to be forgotten are the many associates whose moral support and encouragement sustained me in times of hardship most notably: Dean Nancy Marcus, Dr. Judith Devine, Ms. Dana Zapata and Ms. Lisa Beverly and Mrs. Barbara Johnson. I would like to thank Jerrie Del-Vecchio for encouraging me to pursue graduate studies.

Lastly, but by no means least, honor and glory to Almighty God whose loving kindness and tender mercy have made it possible for me to complete this portion of my education.

TABLE OF CONTENTS

List of Tables	vii
List of Figures	viii
Abstract	x
1.0 INTRODUCTION	1
1.0 The Concept of Solar Energy	1
1.1 Problem Description	3
1.2 Research Objective	4
1.3 Project Rationale and Research Benefits	5
2.0 LITERATURE REVIEW	6
2.0 Introduction	6
2.1 Solar Cell Theory and Basic Formulae	6
2.2 Bandgap and Losses	7
2.3 P/N Junction	9
2.4 Current-Voltage (I-V) Characteristic Curves	10
2.5 Factors Affecting PV Cell Operation	12
2.6 Semiconductor Theory	12
2.7 The Photovoltaic Effect	13
2.8 The (I-V) Characteristic Curve Effect	13
2.9 Solar Spectrum	15
2.10 The Role of Certain Factors on PV Performance	18
2.10.1 Time of day of year	18
2.10.2 Solar irradiation	19
2.10.3 Shading effect	19
2.10.4 The effect of heat on PV module output	19
2.11 PV Cell Material Types	20
2.12 PV Usages in Outdoor Operations	20
2.12.1 The power rating of pv modules	20
2.12.2 The energy rating factor	22
2.12.3 The positioning of pv modules	22
2.12.4 Momentary module output	24
2.12.5 The effect of solar radiation on power output	24
2.12.6 Temperature effect	26
2.12.7 Photovoltaic cell material	27
2.12.8 The silicon group	27
2.13 Photovoltaic Energy Generating Systems	28

3.0 METHODOLOGY	29
3.0 Introduction	30
3.1 Support structure of solar tracker	30
3.1.1 Design and fabrication of tracking system	30
3.1.2 The tracking system	33
3.1.3 Operation of track rack	33
3.2 Preliminary data analysis	36
3.2.1 Types of data collection.....	36
3.2.2 Designed experiment	36
3.2.3 Controllable factors	36
3.2.4 Nuisance factors.....	37
3.2.5 Response variable	38
3.2.6 Experimental setup and choice of experimental design	38
4.0 THE ACTUAL EXPERIMENT	40
4.1 Data collection	40
4.2 Data analysis	42
4.3 Refining the model	51
4.4 Validation	56
4.5 Confirmation	59
5.0 ANALYSIS, RESULTS AND CONCLUDING REMARKS	61
5.1 Recommendations and Future Work	61
APPENDICES	63
REFERNECES	68
BIOGRAPHICAL SKETCH	70

LIST OF TABLES

1. Energy Production in the United States	2
2. Band Gap Semiconductors in PV Devices at Room Temperature	8
3. Conversion Efficiencies of Silicon Materials	27
4. Choice of Factors and Levels for Design of Experiment	37
5. ANOVA Table from Initial Data Analysis	43
6. Second Generation ANOVA Table	45
7. Sample raw data collected from 0 deg, 40 deg and tracker respectively	58
8. Power values and percentage difference between configurations	60
9. Sample Experimental and Transformed Data	64
10. Sample Experimental and Transformed Data (Design Matrix)	65

LIST OF FIGURES

1. Photovoltaic Cell	2
2. Site Map of Location of Solar Tracker	3
3. P/N Junction and Transition Point	9
4. Graph of Maximum Power Point as a Function of Voltage and Current	10
5. Effect of series resistance on IV curve	11
6. Current – Voltage (I-V) Characteristic Curve for a Typical PV Cell.....	14
7. Typical information found on a PV module labels	14
8. Visible light spectrum from ultraviolet to near infrared	16
9. Diagram of PV system with energy storage and grid-connection	21
10. Diagram showing the maximization of irradiant power	23
11. I -V curves of two PV modules	24
12. Diagram showing the inverse of the zenith angle cosine	26
13. Diagram of Market shares of photovoltaic materials	27
14. Complete PV System showing all internal and external components	28
15. Drawing of Winch Assembly and Support Mechanism	30
16. Photo of Completely Assembled Tracking	34
17. Diagram of Tracker Operation 1	35
18. Diagram of Tracker Operation 2	37
19. Fishbone diagram of affecting factors	39
20. Data Collection Using Solar Tracker	41
21. Data Collection in a horizontal Configuration	41

22. Data Collection inclined at an angle of forty degrees.....	42
23. Half Normal Plot of Residuals	43
24. Second Generation Half Normal Plot of Data	44
25. Second Generation Normal Plot of Residuals	45
26. Plot of Residuals vs. Predicted Values	46
27. Plot of Residuals vs. Tracking	48
28. Plot of Residuals vs. Time of Day	47
29. Plot of Residuals vs. Material Type	48
30. Plot of Residuals vs. Inclined Angle	48
31. Plot of Box-Cox Transformation	49
32. Interaction of Mono and Polycrystalline as a Function of Tracking	49
33. Interaction of Mono and Polycrystalline as a Function of Time of Day	50
34. Difference of power between Flat and Tracking	51
35. Refined Half Normal Plot of Mains Effects	52
36. Third Generation Normal Probability Plot of Effects.....	52
37. Third Generation Plot of Residuals vs. Predicted Values	53
38. Third Generation Plot of Residuals vs. Tracking	53
39. Third Generation Plot of Residuals vs. Time-of-Day.....	54
40. Third Generation Plot of Residuals vs. Material Type	54
41. Third Generation Plot of Residuals vs. Inclined Angle	55
42. Third Generation Plot of Predicted vs. Actual Values	55
43. Third Generation Plot of Box-Cox Transformation	56
44. Scatter Plot of Monocrystalline Power Generated at 0°, 40° and Tracking	59

ABSTRACT

The focus of this thesis was to employ the use of two widely used types of photovoltaic (PV) modules namely monocrystalline and polycrystalline in a tracking system to determine which produces the greater output and compare these results to those reached by my predecessor, Michael O. Case[Case, 2003]. Several factors affect the overall productivity of a solar system. These include but are not limited to, time of day, time of year, latitude and atmospheric conditions, all of which were dealt with throughout this thesis.

The thesis began with the design and assembly of a solar tracking system. This system was used to collect data using monocrystalline and polycrystalline modules in various configurations. The configurations were stationary zero degrees, stationary forty degrees and solar tracking at forty degrees.

Once data was acquired, it was entered in to the statistical software “Design Expert V6.0”. Statistical analysis was then performed to determine the effect the chosen factors had on the power output of the two types of modules in terms of which type provides greater output and in what configuration.

It was determined that the monocrystalline module produces greater power output than its polycrystalline counterpart. A final experiment was set up to determine the mode that produces the greatest power output. The results from the experiment revealed that monocrystalline modules deliver greater power in a tracking configuration. However, it may be necessary to consider the effects of temperature depending on application of these modules.

CHAPTER 1

INTRODUCTION

1.0 The Concept of Solar Energy

No concept is more fundamental than that of energy. Energy in its strictest definition is simply the ability to do work and because energy is required to perform work in every sphere of activity, energy is necessary in almost every conceivable form.

One of the more recent additions to the many forms of energy is solar energy. Man has long relied on wood, coal and petroleum as the main source of energy. Also sharing the stage is nuclear energy which, because of its inherent danger, is only suited for limited applications. Due to exhaustion, increasing cost or health and environmental concerns, it is believed that renewable energy such as solar energy will replace conventional sources of energy in the not too distant future.

Photovoltaic cells were first manufactured in the 1950s [FSEC, 2005]. In the early stages of development and testing, they were primarily used to provide electrical power for earth-orbiting satellites. As time progressed and developmental milestones were made, improvements in manufacturing, performance and quality of PV modules drove the price down and gave way to a number of initiatives, including battery charging for navigational aids, signals, telecommunication equipment and other nonessential creature comfort needs requiring low power. Photovoltaic devices gained popularity during the 1980's as the power source of preference for many consumer electronic manufacturers. In the 1990's and into the twenty first century, photovoltaic technology moved from the micro to the commercial macro arena.

PV technology is now being employed at an international level for such purposes as powering residential communities particularly in refrigeration and irrigation. Today, solar energy production is being taken more and more seriously as its low byproduct, inexhaustible characteristics make it more attractive. Furthermore, many international, private, and public research entities are aggressively pursuing photovoltaic power technology and including it in their power generation capacity.

In order to create electrical energy from the sun, the sun's energy must be harnessed in some way. Although there are many ways of capturing the sun's energy, this thesis concentrates

on the use of the theory of photovoltaic technology employed in a single axis tracking system to determine the benefits of monocrystalline over polycrystalline silicone. At the nucleus of the PV module is the PV cell as shown in Figure 1.1. The cell is made of silicon, a special type of melted sand. When sunlight photons strike the solar cell, electrons are knocked loose. They move toward the treated front surface of the cell. An electron imbalance is created between the front and back; and when a connector, like a wire, joins the two surfaces a current of electricity flows between the negative and positive sides.



Figure 1.1 Photovoltaic Cell, the smallest device capable of converting sunlight to direct current electricity.

Table 1.1 Energy Production in the United States [EIA Annual Review, 1998].

COMMODITY	1998 PRODUCTION QUAD BTU ¹	Percent of Total Production	1998 PRODUCTION in NATIVE UNITS ²
Oil	13.2	18.1 %	6.25 MB/D
Natural gas	19.5	26.7 %	18.86 tcf/year
Coal	23.8	32.6 %	1118.7 million short tons
Nuclear	7.2	9.8 %	673.7 billion kWh
Renewable	6.7	9.2 %	75.7 billion kWh
Hydroelectric	3.4	4.7 %	324.1 billion kWh
Other	2.6 (by difference)	3.6 %	
TOTAL	72.9		

¹ EIA Annual Energy Review 1998

² EIA International Energy Annual 1998

1.1 Problem Description

The process of converting radiant solar energy into electrical energy is determined by several factors. This thesis focuses on solar tracking as a means of comparing the output of mono-crystalline and polycrystalline silicon PV modules while giving consideration to the controllable factors such as shading, angle off inclination of tracker, time of day, material type, tracking or nontracking and time of year.

Monocrystalline panels use crystalline silicon produced in large sheets, which can be cut to the size of a module and integrated into the panel as a single large cell. Conducting metal strips are laid over the entire cell to capture electrons in an electrical circuit. Polycrystalline photovoltaics use a series of cells instead of one large cell. These panels (modules) are one of the most inexpensive forms of photovoltaic structures available today, though the costs of sawing and producing wafers can be high. At the same time, they have lower conversion efficiencies than monocrystalline panels.

Figure 1.2 shows the location of the solar tracker as erected on the central eastern side of the Centennial Building, at Innovation Park, Tallahassee, Florida. The module was installed on a latitudinal and longitudinal axis consistent with the geographical location and time of the year when data will be collected.

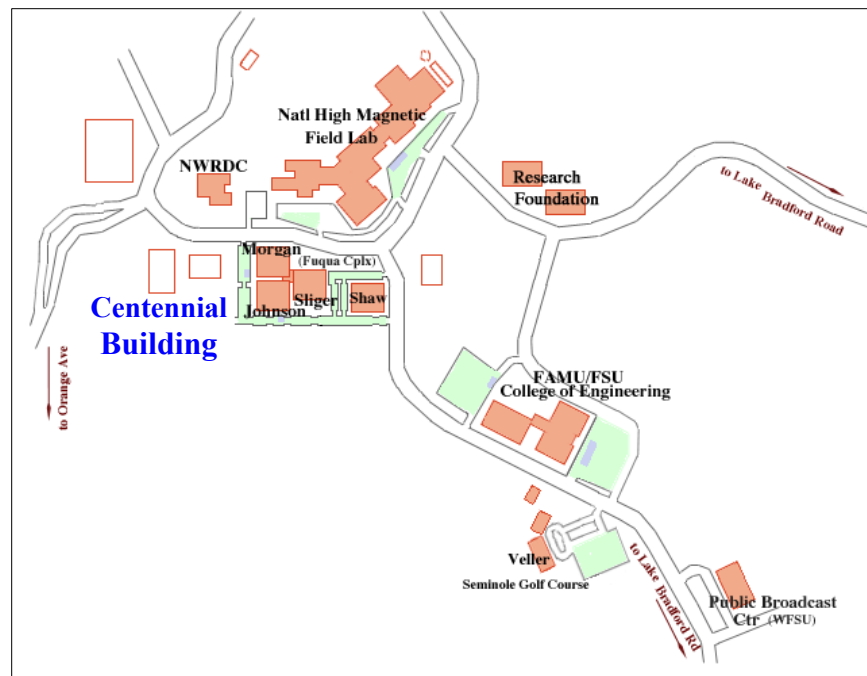


Figure1.1 Site Map of Location of Solar Tracker.

The most common photovoltaic (PV) cell material is silicon. It is one of the most abundant elements on earth: sand from the beach is an oxide of silicon. The first commercial PV cells were monocrystalline silicon. Other manufacturing techniques resulted in polycrystalline silicon cells. A monocrystalline cell is made of a single crystal; a polycrystalline cell contains many crystals. Commercial polycrystalline cells are only slightly less efficient than monocrystalline cells and are, therefore, widely used because their cost-performance ratio is similar [National Solar Power Research Institute, 1998].

The development of thin-film technologies reduces costs further by decreasing the amount of material needed to make a cell. Amorphous silicon modules require only a thin layer of silicon and can be mass-produced. New production techniques led to the manufacture of "multi-junction" amorphous cells, which contain two or three layers of semiconductor. Because of the lower efficiency, modules that are physically larger are needed in order to generate a given amount of power. Other technologies have been developed such as cadmium telluride and copper indium diselenide and these are beginning to appear on the market.

1.2 Research Objective

At present, the efficiency of the monocrystalline and polycrystalline silicon PV modules is between 15-18 and 12-14 percent, respectively. From all indications, these efficiencies were determined from stand alone or stationary mounted modules.

The objectives of the thesis were five-fold:

1. To design and build a solar tracking system.
2. To determine the output of photovoltaic modules through data collection using a data logger and several sensors by tracking the trajectory of the sun as opposed to a stationary arrangement.
3. To test monocrystalline and polycrystalline using the tracking system to determine the percentage increase in output of the modules as a result of tracking.
4. To verify whether the output of tracking system generates at least a 15% increase in efficiency when tracking is employed compared with stationary system.

The testing was carried out considering that most solar testing is done under standard testing conditions which include a solar irradiance of 1000 W/m², spectral distribution of 1.5 AM and at a temperature of 25o Celsius.

1.3 Project Rationale and Research Benefits

The engineering application of this thesis was to design and fabricate a solar tracking system and to calculate the power output of both modules with a view of confirming the potential of increased power output due to solar tracking. This research is justified in as far as it is necessary to maximize on the capturing and conversion of solar irradiance for the purpose of the production of electrical energy. This increases the profitability of using solar as an energy source and reduces the dependence on fossil fuel as the primary energy source.

CHAPTER 2

LITERATURE REVIEW

2.0 Introduction

Energy is the most basic and necessary commodity of all resources. It is essential for existence. Unfortunately, most of the current energy being generated today is heavily dependent on resources that are either growing increasingly expensive, scarce or both.

With the birth of solar energy in the early twentieth century, it has grown in popularity and now has several applications. Solar technology is being employed for electrical energy in remote areas for providing modern conveniences such as refrigeration, heating and cooling and irrigation for rural farming. Most importantly, solar energy is being considered as an alternative to fossil and nuclear energy. The generation of these traditional electrical energy sources versus solar energy presents opposing challenges. The generation of electrical energy from fossil fuel requires close monitoring of the energy conversion process from raw materials such as coal and petroleum. On the other hand, solar radiation energy converted to electrical energy is easily optimized while the conversion process requires minimum monitoring and least pollution during the conversion process.

2.1 Solar Cell Theory and Basic Formulae

Several solid state equations govern the operation principles of solar cells. This chapter on Literature Review explores the most important physical relations surrounding solar cells.

The basic property of semiconductors that make them suitable for photovoltaic applications is their energy band structure. The valence band of any semiconductor is fully occupied at low temperatures, while the conduction band is empty. However, at room temperature the thermal motion of the electrons can excite some electrons to the conduction band. The probability of occupation of an energy state is given by the Fermi-Dirac distribution:

$$f(\varepsilon) = \frac{1}{1 + e^{(\varepsilon - \varepsilon_f)/\kappa T}} \quad 2.1$$

where, $f(\mathcal{E})$ is the occupation probability, \mathcal{E}_F is the Fermi-level energy and T is the Temperature. The density of states for electrons in the conduction band ($g_e(\mathcal{E})$) and holes in the valence band ($g_h(\mathcal{E})$), on the other hand, can be written as [Green, 1982]:

$$g_e(\mathcal{E}) = \frac{8\sqrt{2}\pi m_e^{*3/2}}{h^3} (\mathcal{E} - \mathcal{E}_c)^{1/2} d\mathcal{E} \quad 2.2$$

and

$$g_h(\mathcal{E}) = \frac{8\sqrt{2}\pi m_h^{*3/2}}{h^3} (\mathcal{E}_v - \mathcal{E})^{1/2} d\mathcal{E} \quad 2.3$$

where, m_e and m_h are the effective masses of electrons in the conduction band and holes in the valence band, respectively; and \mathcal{E}_c is the conduction band energy and \mathcal{E}_v is the valence band energy. With the help of equations (2.2) and (2.3), an equation can be derived for the density of electrons in the conduction band, n . In a simplified form this equation can be written as:

$$n = N_c e^{(\mathcal{E}_f - \mathcal{E}_c)/kT} \quad 2.4$$

and the density of holes in the valence band, p , is

$$p = N_v e^{(\mathcal{E}_v - \mathcal{E}_f)/kT} \quad 2.5$$

where, N_c and N_v are the so-called effective densities of states in the conduction band and valence band, respectively. Equations (2.4) and (2.5) are valid both for pure and doped semiconductors, even though the Fermi level is shifted in the latter. The study of current transport in solar cells is based on the transport equations of 2.4 and 2.5, the continuity equations and the Poisson equation. The system is essentially one-dimensional as far as current transport is concerned, so all variables are functions only of y , the coordinate through the cell [Green, 1982].

2.2 Bandgap and Losses

Impinging photons can excite electrons from the valence band to the conduction band if

the energy gap E_g is narrow enough. The movement of an electron also creates a hole in the valence band, which acts like a charge carrier. If a meaningful voltage is to be sustained in the material, the energy gap also needs to be wide enough to prevent the immediate recombination of the generated electrons and holes before they can be separated. The bandgaps of the most widely used photovoltaic materials at room temperature are presented in Table 2.1.

Aside from the width of the bandgap, the electron excitation probability also depends to a large degree on whether the bandgap is direct or indirect. Light absorption in *Si* is much less efficient than in *GaAs*, *CdTe* and *CIS* because *Si* has an indirect bandgap, while the other three have direct bandgaps.

Table 2.1 The Band Gap of the most frequently used Semiconductors in Photovoltaic Devices at Room Temperature.

Material	<i>Si</i>	<i>GaAs</i>	<i>CdTe</i>	<i>CIS</i>
Bandgap	1,1 eV	1,4 eV	1,5 eV	1,0 eV

Photons with wavelengths shorter than approximately 800-850 nm can excite electrons to the conduction band in the semiconducting materials presented in Table 2.1. However, photons with high energies do not produce a higher photovoltage than low-energy photons, since excited electrons quickly sink to the bottom of the conduction band, and the excess energy is dissipated as heat. The energy which can be generated is thus in theory always equal to the bandgap energy of the material. In practice it is smaller than the bandgap, since the p/n-junctions which separate charge carriers in a solar cell are not capable of converting the entire bandgap to output energy. There are thus three inherent energy loss mechanisms which are always present in photovoltaic devices, namely:

1. Photons with energies larger than the bandgap excite electrons to the conduction band, but any excess energy is lost when the electron thermalizes to the bottom of the conduction band.

2. Photons with too little energy can not excite electrons to the conduction band, and their energy is therefore lost.
3. Only a part of the bandgap energy (about 60% for c-Si solar cells) can be converted to output energy in the p/n-junction. These loss mechanisms are some of the most important factors, which significantly lower the theoretical maximum efficiency of solar cells [Green, 1982].

2.3 P/N Junction

When an electron is excited to the conduction band by a photon, it eventually recombines with a hole in the valence band unless the two are separated. This means that an electric field which drives electrons and holes in opposite directions must be present in the semiconductor if the energy of the photons is to be taken advantage of. This electric field can be created in a *p/n-junction* by joining an “n”- type semiconductor to a “p”- type semiconductor. The base materials (i.e. the semiconducting materials) can either be the same on both sides of the junction (as in *Si* cells), or they can be different in other types of materials. The n-type material has been doped with atoms containing one extra electron, while the p-type material contains atoms with one electron less than the base material. The p/n junction is presented graphically in Figure 2.1. The Fermi levels of the ‘p’- type material is close to the valence band, while the n-type Fermi level is close to the conduction band. When the two materials are joined together, the Fermi energy must be equal on both sides of the junction, which results in the bending of the energy bands and the creation of an electric field across the junction. By connecting the p- and n-sides to an external circuit or a load, this photo current can be utilized.

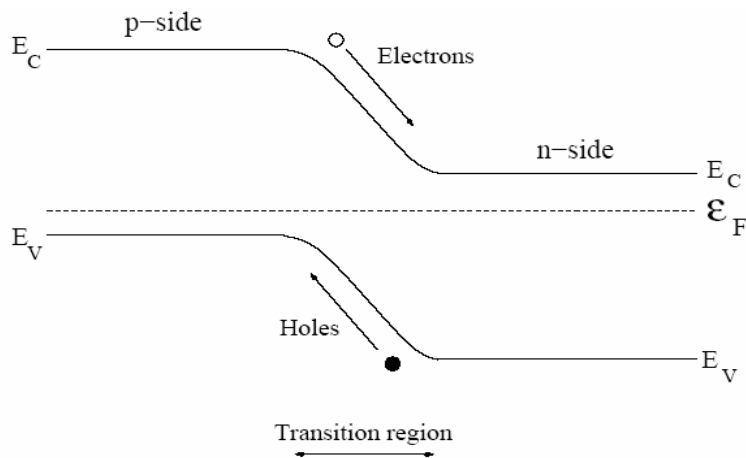


Figure 2.1 P/N Junction and Transition Point.

2.4 Current-Voltage (I-V) Characteristic Curves

By studying the transport equations of the charge carriers in the transition region, a supposed ideal diode law can be derived for a p/n-junction in the dark, when no charge carriers are generated by sunlight. This law is written as:

$$I = I_0(e^{qv/k_B T} - 1) \quad 2.6$$

where, I is the diode current, I_0 is the so-called saturation current, q is the elementary charge, V is the diode voltage and T is the temperature. When illumination is taken into account, the equation is modified into [Green, 1982]:

$$I = I_0(e^{qv/k_B T} - 1) - I_L \quad 2.7$$

where I_L is the light-generated current. Equation 2.7 determines the current-voltage relationship of an ideal solar cell with $R_s = 0$ and R_{sh} approaches infinity. The I-V curves corresponding to equations (2.6) and (2.7) have been plotted in Figure 2.2.

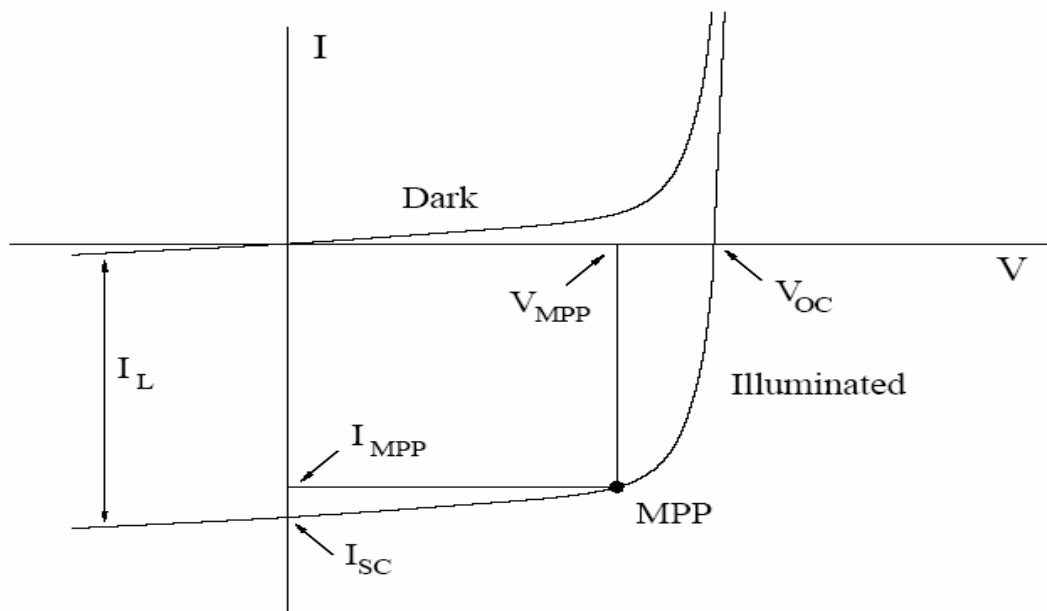


Figure 2.2 Graph of Maximum Power Point as a Function of Voltage and Current.

The I-V curve of an illuminated p/n-junction is simply the dark I-V curve shifted downwards by the light-generated current I_L . The open-circuit voltage V_{oc} and the short circuit current I_{sc} are found where the curve crosses the axes and maximal power can be extracted from the solar cell at the point (V_{MPP}, I_{MPP}) .

The I-V curve of a real solar cell with series and shunt resistances is shifted closer to the origin of the coordinate system. Large values of R_s cause the current values to become smaller, while small values of R_{sh} reduce the voltage, as seen in Figure 2.3. Loss mechanisms also usually make the I-V curve flatter, and the so-called fill factor (FF) is a measure of this flatness. It is defined as:

$$FF = \frac{V_{MPP} * I_{MPP}}{V_{OC} * I_{OC}} \quad 2.7$$

The fill factor corresponds to the ratio between the produced power and the power in the ideal case where the I-V curve has a rectangular shape with no losses. The fill factor, the efficiency and the I-V curve parameters are very important in the study of photovoltaics, because their values essentially reveal how well a device is working.

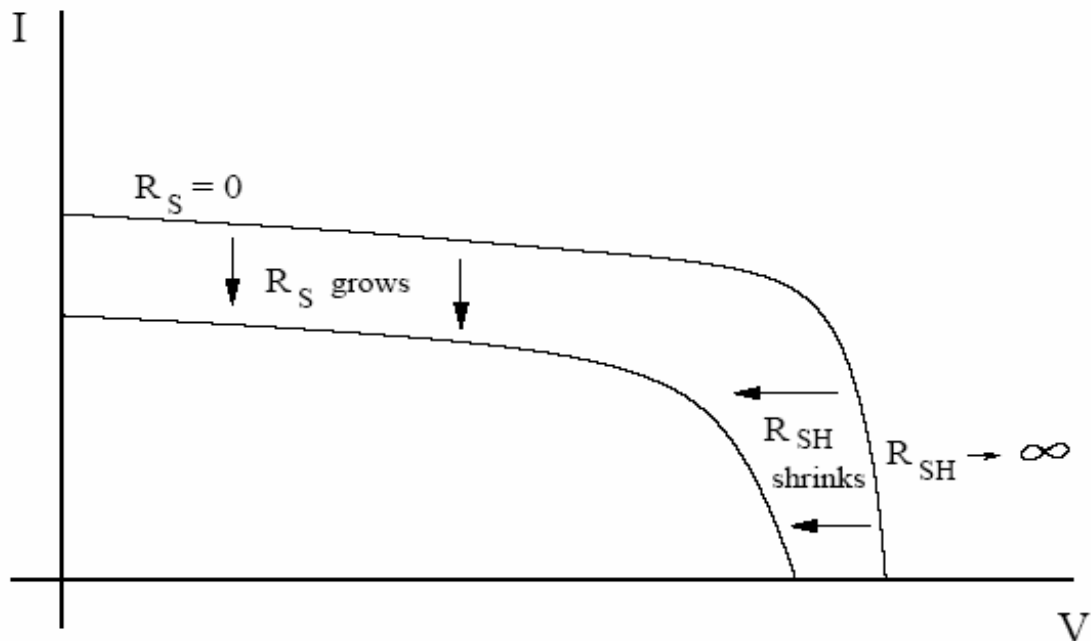


Figure 2.3 Effect of series resistance on IV curve -Large Values for the Series Resistance R_s shift the I-V curve lower along the Current axis, while small values for the Shunt Resistance R_{sh} shift it to the left along the Voltage axis.

2.5 Factors Affecting PV Cell Operation

Solar energy, power from the sun, is free and inexhaustible. In the broadest sense, solar energy supports all life on earth and is the basis for almost every form of energy currently being used. The sun makes plants grow, which are burned as fuel or rot in swamps and are compressed underground for millions of years to become coal and oil. Heat from the sun causes temperature differences between areas, causing the wind to blow. Water evaporates because of the sun, falls on high elevations, and rushes down to the sea, spinning turbines as it passes. But solar energy usually refers to ways this energy can be used as heat, lighting, and electricity. The amount of energy from the sun that falls on the earth is enormous. All the energy stored in the earth's reserves of coal, oil, and natural gas is matched by the energy from 20 days of sunshine. Outside the earth's atmosphere, the sun's energy contains about 1,300 watts per square meter. About one-third of this light is reflected back into space, and some is absorbed by the atmosphere.

By the time it reaches the earth's surface, the energy in sunlight has fallen to about 1,000 watts per square meter (regarded as the solar constant), at noon on a cloudless day. Averaged over the entire surface of the earth, 24 hours per day for a year, each square meter collects about the energy equivalent of a barrel of oil. So each day, on average, a square meter collects 4.2 kilowatt-hours of energy. This number varies by location and by weather patterns. Deserts, with very dry air and little cloud cover, receive the most sun, more than 6.0 kilowatt-hours per day per square meter. Northern climates, such as that of Boston, get closer to 3.6 kilowatt-hours. Sunlight varies by season as well, with some areas receiving very little sunshine in the winter. Seattle in December, for example, gets only about 0.7 kilowatt-hours per day. This solar resource is the maximum available to be captured and used for energy [M.I.T. Press, 1992].

2.6 Semiconductor Theory

Solar cells compose various semi-conducting materials. Semiconductors are materials, which become electrically conductive when supplied with light or heat, but which operate as insulators at lower temperatures.

Over 95% of all the solar cells produced worldwide are composed of the semiconductor material silicon (Si). As the second most abundant element in the earth's crust, silicon has the advantage of being available in sufficient quantities, and additionally processing the material

does not burden the environment. To produce a solar cell, the semiconductor is contaminated or "doped". "Doping" is the intentional introduction of chemical elements, with which one can obtain a surplus of either positive charge carriers (p-conducting semiconductor layer) or negative charge carriers (n-conducting semiconductor layer) from the semiconductor material. If two differently doped semiconductor layers are combined, then a so-called p-n-junction results on the boundary of the layers.

At this junction, an interior electric field is built up which leads to the separation of the charge carriers that are released by light. Through metal contacts, an electric charge can be tapped. If the outer circuit is closed, meaning a consumer is connected, and then direct current flows.

Silicon cells are approximately 10 cm by 10 cm large (recently also 15 cm by 15 cm). A transparent anti-reflection film protects the cell and decreases reflective loss on the cell surface.

2.7 The Photovoltaic Effect

The "photovoltaic effect" is the basic physical process through which a solar cell converts sunlight into electricity. Sunlight is composed of photons--packets of solar energy. These photons contain different amounts of energy that correspond to the different wavelengths of the solar spectrum. When photons strike a PV cell, they may be reflected or absorbed, or they may pass right through. The absorbed photons generate electricity.

The energy of a photon is transferred to an electron in an atom of the semiconductor device. With its newfound energy, the electron is able to escape from its normal position associated with a single atom in the semiconductor to become part of the current in an electrical circuit. Special electrical properties of the PV cell a built-in electric field provide the voltage needed to drive the current through an external load.

2.8 The (I-V) Characteristic Curve Effect

The PV module operates at any combination of current and voltage found on its "I-V characteristic curve." But in reality it operates at only one combination at a given time. This favored combination is chosen not by the modules, but rather by the electric characteristics of the circuit that is connected to the modules. The voltage that occurs when current is zero is known as the open-circuit voltage (V_{oc}). On the other hand, the current when the voltage is zero is referred to as the short-circuit current (I_{sc}).

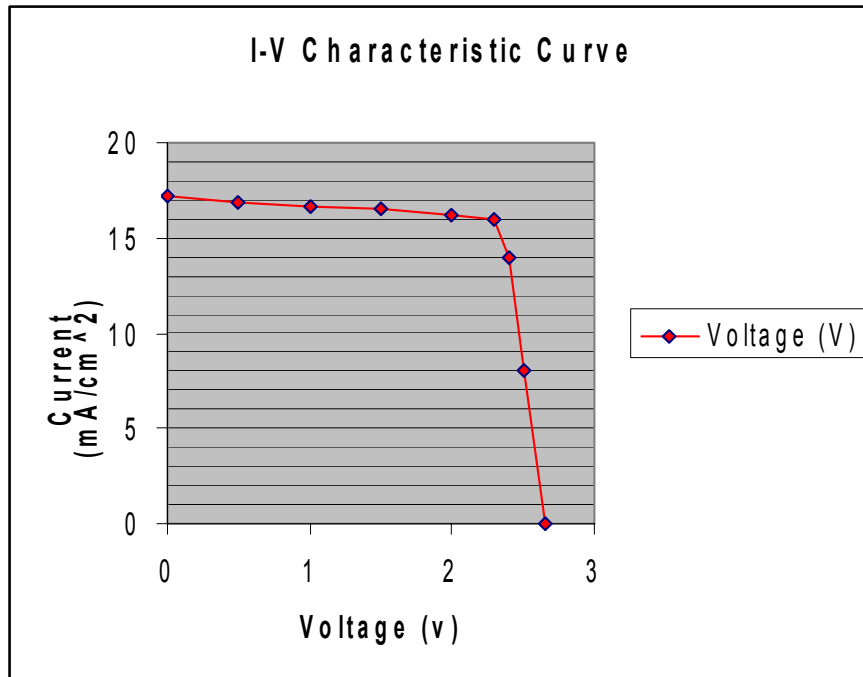


Figure 2.4 Current – Voltage (I-V) Characteristic Curve for a Typical PV Cell.

While current and voltage are at their highest under short-circuit and open-circuit conditions, respectively, the power at these points is zero. In practice, a system operates at a combination of current and voltage at which a reasonable amount of power is produced. The best point is the maximum power point (MPP) which corresponds to nominal voltage (V_p) and nominal current (I_p). This point of operation (MPP) is used to define the nominal rating and efficiency of a module. Figure 2.6 shows typical information (data) found on PV module labels.

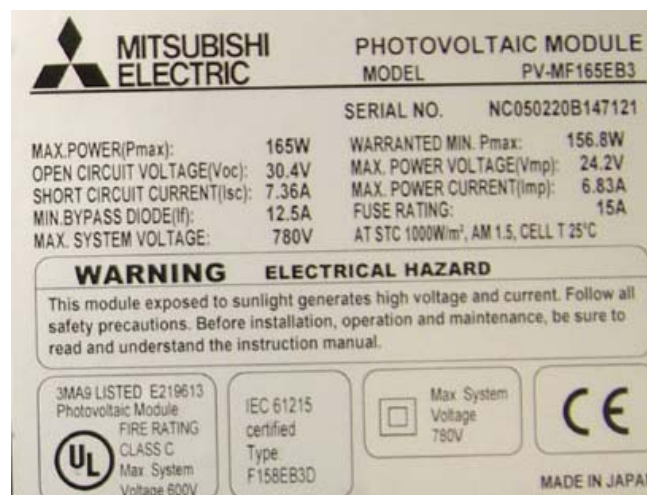


Figure 2.5 Typical Information Found on a PV Module Labels

All the electric characteristics (V_{oc} , I_{sc} , MPP, V_p , I_p) can be found on the label of a good-quality PV module (note that the V_p and I_p values are also called nominal or rated voltage and current). The rated power is seldom obtained from the installed system. It is impossible for a fixed module to operate at the highest power point at all times since the incident rays from the sun is fixed per day on its trajectory. A tracking module has multiple incident rays as it tracks the sun's movement in the sky. Temperature variations alone will change the amount of power a system generates.

2.9 Solar Spectrum

Solar radiation is a general term for the electromagnetic radiation emitted by the sun. This radiation can be captured and converted here on the Earth to useful forms of energy such as heat and electricity, using a variety of technologies. The technical feasibility and economical operation of these technologies at any specific location is dependent on the nature of the solar resource.

Solar radiation has a spectral or wavelength distribution from short wavelength radiation (Gamma-rays and X-rays) to long wavelength radiation (long radio waves). The range of their wavelengths can describe the different regions of the solar spectrum, as shown in Figure 2.6. The combined radiation in the wavelength region from 280 nanometers (one billionth of one meter) to 4,000 nm is called the broadband or total solar radiation. About 99 percent of solar radiation is contained in the wavelength region from 300 nm to 3,000 nm. The region of the spectrum that is visible to humans (sunlight) extends from about 390 nm (ultraviolet) to 780 nm (near-infrared), and makes up only about 10 percent of the total solar spectrum. However, it is the most practically useful part of the spectrum for humans (and most other life on the planet). This is because the wavelengths of the solar spectrum also correspond to different energy levels. Short-wavelength radiation has a higher energy level than long-wavelength radiation.

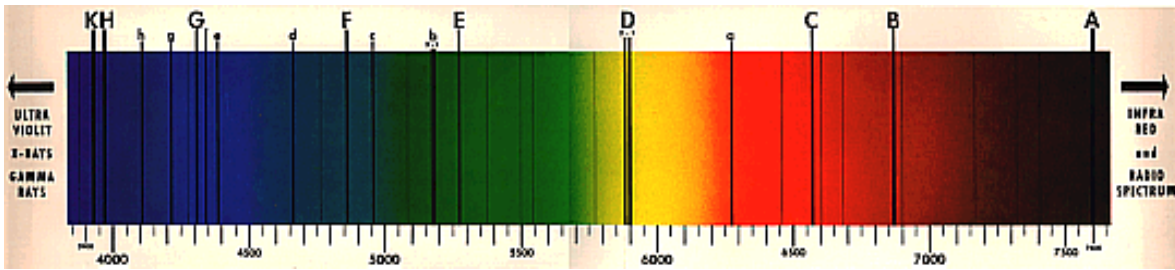


Figure 2.6 Visible Light Spectrum from Ultraviolet to Near Infrared.

The rate at which solar radiation strikes earth's upper atmosphere is expressed as the "solar constant." This is the average amount of energy received in a unit of time on a unit of area perpendicular to the sun's direction at the mean distance of the earth from the sun; 92,960,000 miles (149,604,970 kilometers). While the distance between the earth and the sun varies as the earth moves around the sun on its elliptical orbit, the variation in the distance does not have a significant effect on the amount of solar radiation reaching the earth. The earth is closest to the sun in late December/early January and farthest from the sun in late June/early July. The average intensity of solar radiation reaching the upper atmosphere is about 1,367 watts per square meter (W/m^2) or 434 British Thermal Units (Btu) per square foot.

The amount of this energy that reaches any one "spot" on the earth's surface will vary according to atmospheric and meteorological (weather) conditions, the latitude and longitude of the spot and local landscape features that may block the sun at different times of the day. As sunlight passes through the atmosphere, some of it is absorbed, scattered, and reflected by air molecules, water vapor, cloud cover, dust, and pollutants from power plants, forest fires, and volcanoes. This is called diffuse solar radiation. The solar radiation that reaches the surface of the earth without being diffused is called direct beam solar radiation. The sum of the diffuse and direct solar radiation is called global solar radiation. Atmospheric conditions can reduce direct beam radiation by 10 percent on clear, dry days, and by 100 percent during periods of thick clouds [King et al, 1998].

The daily rotation of the earth and its seasonal movement on its axis has significant implications for practical use of solar energy. For any spot on the earth's surface, the amount of energy it receives will vary on an hourly, daily, and seasonal basis. It is the angle of the sun's position in the sky relative to a point on the earth's surface that determines the intensity of

sunlight reaching that spot. The lower the sun appears in the sky, the more of the earth's atmosphere that the sunlight passes through before it reaches the surface, and the more it is diffused.

Direct solar radiation is generally most intense at any one spot on the surface of the Earth at solar noon, the time at which the position of the sun is at its highest elevation in the sky. At this time, the sun is either due South (typically in the Northern Hemisphere) or due north (typically in the southern hemisphere). This time can be quite different from noon according to local standard time, since it is most perpendicular in the sky, and has the least amount of the atmosphere to travel through. For locations at and north of 23.5 degrees north latitude, it is most intense at solar noon on the 21st June (the summer solstice). At that time, the sun is at the highest point in the sky that it will reach during the year, and it is at this point that sunlight passes through the least amount of the earth's atmosphere. The summer solstice is also the longest day of the year. For these same locations, the shortest day of the year, and the day when sunlight is the least intense is the 21st December (the winter solstice). The opposite is true for locations in the southern hemisphere. Higher latitudes have more hours of sunlight in the summer and less hours of sunlight in the winter relative to lower latitudes. For a point on the equator, the sun will be most intense around the 20th and 21st March and September, respectively, (the spring and vernal equinoxes) as these are the days when the sun is directly overhead.

Solar collectors can be positioned to maximize the amount of solar energy that they receive on a daily and seasonal basis. In general, the optimum orientation of a solar collector is directly true south (in the northern hemisphere; true north in the southern hemisphere). However, local landscape features, such as trees, buildings, and hills or mountains may shade a solar collector during different times of the day during different seasons. Local weather conditions, such as typically foggy mornings or cloudy afternoons, may also affect the optimum orientation. In these situations, the orientation may be east or west of south to optimize solar energy reception daily and/or seasonally.

The angle of a solar collector relative to sun's position in the sky also greatly affects the amount of solar energy it receives. For example, a flat, horizontal surface facing true south in Topeka, Kansas (at 39 degrees North), with total exposure to the sun all day throughout the year, will receive an annual average of 4.3 kilowatt-hours (KWh), or 12,969 Btu, per square meter (10.76 square feet) per day, while a vertical surface will receive 3.3 kWh (10,239 Btu) per square

meter per day. In July, the horizontal surface will receive 6.6 kWh (22,526 Btu) per square meter per day and the vertical surface will receive 2.6 kWh (8,874 Btu), because the sun is higher in the sky in the summer and strikes the horizontal surface more directly. When the sun is lower in the sky in December, the horizontal surface will receive 1.9 kWh (6,485 Btu) per day, while the vertical surface will receive 3.4 kWh (11,604 Btu) [National Renewable Energy Lab, 2000].

For solar collectors where the angle is fixed (such as low-temperature, flat-plate water or space heaters) an optimum angle must be selected. The general rule of thumb is that for maximum solar reception during winter months, the optimum angle is the angle of latitude plus 15 degrees. For maximum solar reception in summer months, the optimum angle is the angle of latitude minus 15 degrees. For latitudes at or near the tropics, no adjustment is necessary. The angle at which the sun's rays strike the earth's surface hardly changes; hence adjusting the angle of the solar module can be counterproductive.

Some types of solar energy conversion systems use tracking devices that position a solar collector to face the sun. A tracking system is necessary for solar energy systems that concentrate sunlight onto an absorber. Concentrating solar collectors use primarily direct beam solar radiation. Flat-plate collectors (in fixed positions and on trackers) can use direct beam and diffuse radiation, and even radiation reflected off the ground or surrounding objects and fixed reflectors [Carlsson, 2001].

2.10 The Role of the factors on PV performance

Several factors influence how well PV panels perform. Some of these factors are time of year, solar irradiation, shading effect, temperature and material type.

2.10.1 Time of day of year. The intensity of solar radiation varies significantly over the course of a year ranging from no solar radiation during the polar winter to a maximum of 350 to 400 watts per square meter (W/m²) in the summer. Over the course of a day, the sun's angle above the horizon (solar altitude) influences the intensity of solar radiation: the noon sun is more intense than the rising or setting sun. The maximum altitude of the sun depends on time of year and latitude. However, during the polar winter the sun is below the horizon for 24 hours, and there is no solar radiation, while at midsummer the sun changes little in altitude over the course of a day.

2.10.2 Solar irradiation. Power of a solar cell changes with solar radiation, which is different for different geographical locations, tilt angles and orientations. The change of power is

almost linear with the solar radiation. There is a very little change in open circuit voltage (V_{oc}) of the solar cell, but the short circuit current (I_{sc}) varies almost linearly with the solar intensity.

2.10.3 Shading effect. Shading has a very bad impact on the performance of the PV system. Even partial shading (on one or two cells) of the whole module can reduce the output drastically and if it persists for a longer period, it may damage the whole system. To protect the modules from such adverse effect, a bypass diode is used. The effect is more prominent in crystalline silicon solar modules. Amorphous silicon modules are less affected by shading.

2.10.4 The effect of heat on PV module output. A PV module's power output is reduced at high temperatures, but the lifetime of the PV module (estimated to be at least 20, maybe 30 years) is not affected by normal outdoor heat.

The duration of sunlight and the intensity of the sunlight have a major effect on the output of a PV module, and the increase in temperature has a lesser effect on the output. Therefore, a PV module installed in Arizona will put out much more energy over a year than an exact same module installed in Boston, Massachusetts. The Boston module does not get as hot, and would put out slightly more power when at peak (around noon time) conditions, but the module in Arizona will get about 70 percent more sunlight energy in, and will only lose about 20 to 30 percent due to the increase in operating temperature. This is an overall gain of 40 to 50 percent.

A general "rule of thumb" for crystalline silicon PV modules (the most common type to date) is that the efficiency (and, therefore, the power output) is reduced about 0.5 percent for every degree Celsius increase in temperature. PV modules are usually rated at module temperatures of 25°C (77°F) and seem to run about 20°C over the air temperature. So on your hot day of 100°F, the module will be 120°F or 50°C, so it will have its power reduced by 12.5 percent. The design of a PV system usually takes into consideration the need to allow some "convective cooling" for the PV modules, that is, some way to passively dissipate the heat generated from the module and minimize the module temperature to increase the performance. The usual method is to leave the back open and allow some airflow around the modules [Solar Electric Power Association, 2000].

2.11 PV Cell Material Types

PV cells are made of semiconductor materials. The major types of materials are crystalline and thin films, which vary from each other in terms of light absorption efficiency,

energy conversion efficiency, manufacturing technology and cost of production. Single-crystal silicon cells are the most common in the PV industry. The main technique for producing single-crystal silicon is the Czochralski (CZ) method.

High-purity polycrystalline is melted in a quartz crucible. A single-crystal silicon seed is dipped into this molten mass of polycrystalline. As the seed is pulled slowly from the melt, a single-crystal ingot is formed. The ingots are then sawed into thin wafers about 200-400 micrometers thick (1 micrometer = 1/1,000,000 meter). The thin wafers are then polished, doped, coated, interconnected and assembled into modules and arrays.

Consisting of small grains of single-crystal silicon, polycrystalline PV cells are less energy efficient than single-crystalline silicon PV cells. The grain boundaries in polycrystalline silicon hinder the flow of electrons and reduce the power output of the cell. The energy conversion efficiency for a commercial module made of polycrystalline silicon ranges between 10 to 14% [Zweibel, 1990].

2.12 Photovoltaic Usage in Outdoors Operations

Photovoltaic power sources are set apart from traditional ones by their dependence on time of day and season. This brings about the important issues related to the use of PV modules, beginning with the definition of the output power and the effect which different environmental variables have on modules.

2.12.1 The power rating of PV modules. Since sunlight is by its very nature an intermittent energy source, photovoltaic modules have to operate under conditions that may vary greatly from one moment to the next. This places certain restrictions on their use, because they cannot produce energy at a constant rate. In practice, this means that an autonomous PV system functioning as the only power supply for a house cannot be connected directly to electric appliances. With the help of various solutions for energy storage, such as the use of batteries, the variability of a PV module's energy output can be "leveled off" to obtain a steady supply of power. In grid-connected applications, where the PV system supplies only part of the power for the household, the power from the modules can be used more directly. A schematic presentation of a PV system with energy storage and grid-connection is shown in Figure 2.7.

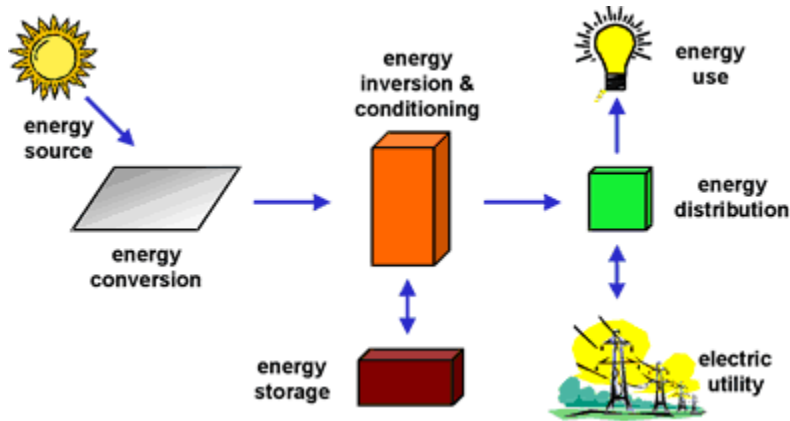


Figure 2.7 Diagram of PV system with energy storage and grid-connection.

The variations in energy output also lead to questions on how the power of a photovoltaic module should be defined in the first place. Average power output cannot be given directly, because it depends to a great degree on the location and weather conditions of the site at which it will be used. Therefore, it is common practice that a photovoltaic module's power is given as a peak value P_p , whose unit is often designated by W_p (peak watts). The peak power corresponds to the power output under a solar irradiance of 1000 W/m^2 incident directly on the surface of the module at a module temperature of 25°C . The nominal peak power ratings are given to PV modules with the help of solar flash simulators. These simulators illuminate a module for a very short time with an irradiance of 1000 W/m^2 , and measure its response. The solar irradiance value of 1000 W/m^2 corresponds to the irradiance on a very bright and sunny day, which has to be emphasized when PV modules are sold. A certain amount of installed MW_p capacity will produce significantly less power than the rated value.

2.12.2 The energy rating factor. In order to avoid some of the problems mentioned in the previous section, the concept of an "energy rating factor" R_E must be introduced. This factor is derived from long-term experimental outdoor tests at different locations. It is defined as

$$R_E = \frac{U_p}{P_p t_p} \quad 2.1$$

where, P_p is the peak power, T_p is the number of hours that the sun is in 'peak' position

during a specified time period, and Up the energy delivered by the module during the same time period. The peak hour time Tp corresponds to the hours of the day when the sun is shining on the module without clouds or any other obstructions in the way. In practice, this means that the solar irradiance exceeds a certain lower limit during these peak hours.

Both Up and Tp depend on the location and time of year, but their ratio remains almost constant, so R_E should be approximately constant as well. Since different climates have their own characteristics, R_E may in practice be calculated for locations at certain latitudes, with clear views of the sky.

The energy-rating factor is one of the most important parameters that researchers seek to determine when PV modules are tested in the field. If the energy rating factor is close to the value 1, then the module has been rated well, and should live up to the customer's expectations. Having values smaller than the number 1 indicate that the module power has possibly been rated for a different climate than the one at the test site, and would therefore perform worse than the customer expects in these conditions. Thorough evaluation of the energy rating factor enables an adjusted power rating which best represents the weather conditions at hand [Fukae et al, 1996].

2.12.3 The Positioning of PV Modules. The power output of a photovoltaic module also depends to a large degree on the angle of incidence of sunlight, denoted by θ . This angle is defined as the angle between the normal of the module plane and the rays of light, as shown in Figure 2.7. The energy flux incident in the surface of the module E_p , is given by the perpendicular component of the total flux. The more descriptive term 'energy flux' is a synonym for the term "solar irradiance" and it is given as:

2.2

$$E_p = E \cos \theta$$

where E is the total energy flux from the angle θ , see Figure 2.7. The module therefore receives a maximal power input when sunlight hits it at a right angle and $\theta = 0^0$. The power produced by the PV module, P , can be written as

$$p = E_p \eta A = E \cos \theta \eta A \quad 2.3$$

where η is the efficiency of the module and A is its area. The perpendicular component E_p of the irradiance determines module output. The best tilt angle Φ depends, among other things, on the latitude of the site in question and the time of year when maximum performance is required.

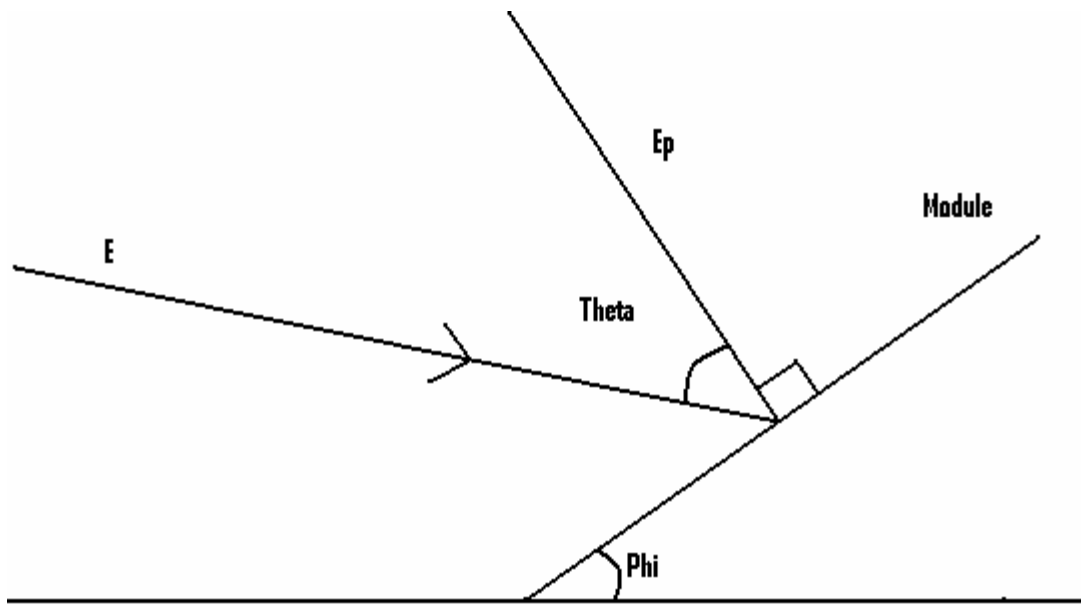


Figure 2.8 Diagram showing the maximization of irradiant power.

The best power production over an entire day for PV modules in a fixed orientation is obtained with modules facing southwards (in the northern hemisphere). The choice of the tilt angle Φ depends to a large degree on the time of year when optimum performance is required. A small tilt angle gives maximal power in the summer (when the position of the sun appears high in the sky), while a larger tilt angle results in better performance during spring and autumn. In residential applications, where PV modules are integrated into the facades or roofs of buildings, the positioning has to be optimized to satisfy the constraints posed by the environment as well. Some of the difficulties related to the fixed mounting of PV modules can be avoided by the use of sun-tracking devices, which are automated devices designed to point directly towards the sun at all times, thus keeping θ close to zero and giving a higher power output. However, the change is warranted only if the increase in power output (compared to the power of fixed modules) is significant, and for this purpose the trackers are also often equipped with concentrating mirrors.

These mirrors reflect sunlight from a larger area onto the module, thereby creating a higher solar irradiance on the module than the standard sea-level value of 1000 W/m^2 . This increases the power output significantly. The downside of concentrating trackers is that they are

quite expensive, and these solutions are therefore only applicable to a limited amount of PV applications.

2.12.4 Momentary module output. Although the power output of a module integrated over long periods of time can be approximated with the help of quantities such as the peak power and the energy rating factor, the power delivered at a certain instant is still very much a function of the weather conditions at hand. Two parameters, which are especially critical, are the solar irradiance and the temperature of the module.

2.12.5 The effect of solar radiation on power output. The solar irradiance (hereafter simply called *irradiance*) is naturally the first and foremost variable that needs to be considered, since it directly dictates how much energy the module can deliver. The total radiative energy received from the sun on an overcast day can be as little as a quarter of the input energy obtained on a clear and sunny day, which clearly illustrates how much the irradiance changes daily. The most pronounced effect of the irradiance is that it determines the number of charge carriers in the active material, mathematically represented by Figure 2.6. This is illustrated in Figure 2.9, which shows two I-V curves of a Siemens ST40 CIS photovoltaic module. The upper curve was obtained with a direct irradiance of 800 W/m^2 , while the lower curve corresponds to 400 W/m^2 . The light-generated current is approximately twice as large on the upper as it is on the lower [http://www.sandia.gov/pv/, October, 2001].

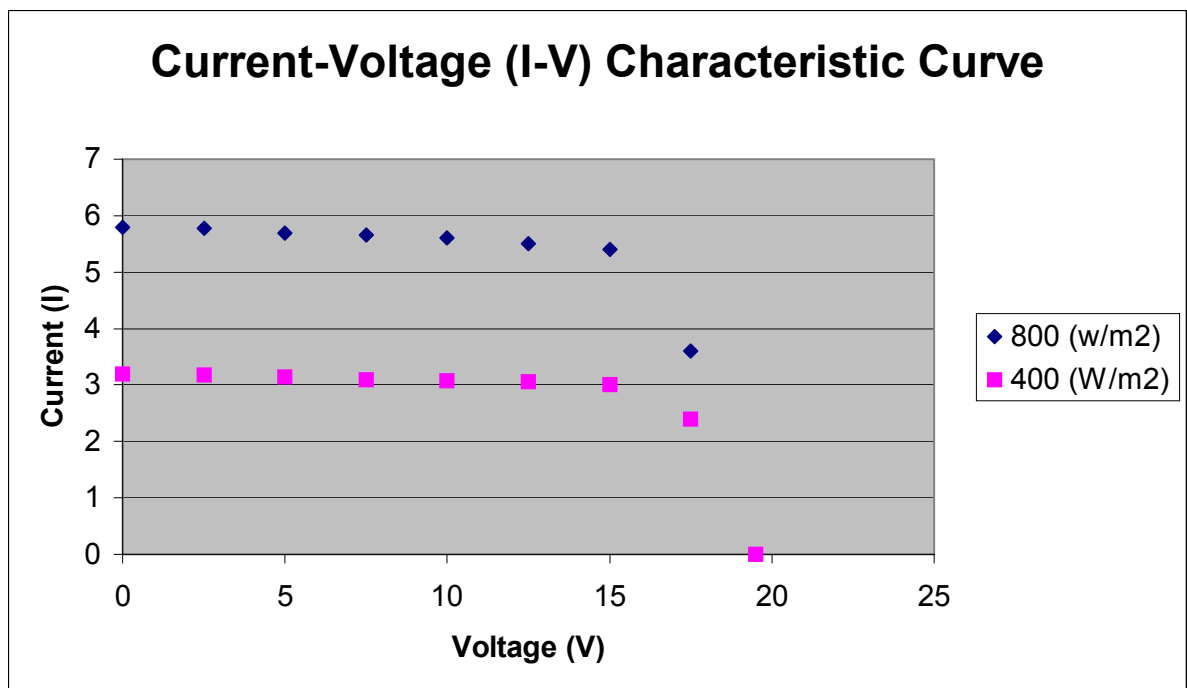


Figure 2.9 I-V curves of two PV modules.

In Figure 2.8, the irradiance determines the light-generated current I_L , and thus the height of the I-V curve. The two curves correspond to a direct irradiance of 800 W/m^2 , 400 W/m^2 , respectively.

The spectral distribution of the incident radiation also plays a role in determining how the module performs, and different solar cells differ in their ability to absorb a wide spectrum. The monochromatic directional absorbance α_λ of a material is equal to the fraction the material absorbs of incident monochromatic irradiance with wavelength λ :

$$\alpha_\lambda(\theta) = \frac{E_{abs,\lambda}(\theta)}{E_\lambda(\theta)} \quad 2.4$$

where, $E_{abs,\lambda}$ is equal to the absorbed irradiance at wavelength λ , and E_λ is the incident irradiance at the same wavelength. The θ dependence shows that α_λ depends on the direction of the incident irradiance, and it also depends on the thickness of the material. The radiance absorbed over all wavelengths from all directions can be written as

$$E_{abs} = \iint_{\lambda,\theta} \alpha_\lambda(\theta) E_\lambda(\theta) d\lambda d\theta \quad 2.5$$

Where, E_{abs} is the total absorbed irradiance and the integration is performed over all possible values of λ and θ . At any given moment, the values of the functions E_λ depend directly on the Air Mass (AM) value, which is defined as the “number of atmospheres” the light travels through on its way to the module. The base value of AM is 1, which corresponds to a situation where the light comes directly from above, and penetrates ‘one atmosphere on its way down. In Figure 2.10, where the atmosphere thickness has been marked as L , shows that the AM value is approximately proportional to the inverse of the zenith angle cosine.

The irradiance is attenuated in the atmosphere according to an exponential law, which can be written as

$$E(l) = E_{ET} e^{-k \frac{l}{\cos(\theta_z)}} \quad 2.6$$

where $E(l)$ is the irradiance at a distance l from the atmospheric boundary, E_{ET} is the extraterrestrial irradiance, k is the attenuation coefficient and θ_z is the zenith angle. This formula applies to all wavelengths of radiation, although different wavelengths may have different attenuation coefficients. A value of 1.5 for the Air Mass is used to define the reference spectrum for sunlight, and it corresponds to a zenith angle close to 45° . Also having direct consequence on

solar module performance is the Air Mass value. Defined as the amount of atmosphere of thickness l sunlight penetrates on it was down to the earth's surface and is given by the inverse cosine of the zenith angle; the angle of incidence of sunlight on the module. Due to the optical properties of the glass, high angles of incidence usually lead to more reflection losses on the surface of the module than low angles do, so the performance of a module is affected by this phenomenon as well.

2.12.6 The temperature effects. The temperature dependence of the IV-curve is found in its formula, equation (2.7) for the diode current:

$$I = I_0(e^{qv/k_B T} - 1) \quad 2.7$$

which shows that the diode current decreases with increasing temperature T if voltage V remains constant? However, I_{sc} is not a direct function of temperature, since it is obtained when the exponent is zero ($V = 0$). It can be shown that the voltage of a solar cell is more sensitive to temperature changes than the current. The module temperature also affects the band gap of the semiconducting material and the series resistance R_s . The magnitude of the effect depends on the photovoltaic material in question. The irradiation, the ambient temperature, and the wind speed at the site determine the temperature of a PV module in the field. For most technologies, a low module temperature is favorable, since it usually gives both a higher current and a higher voltage.

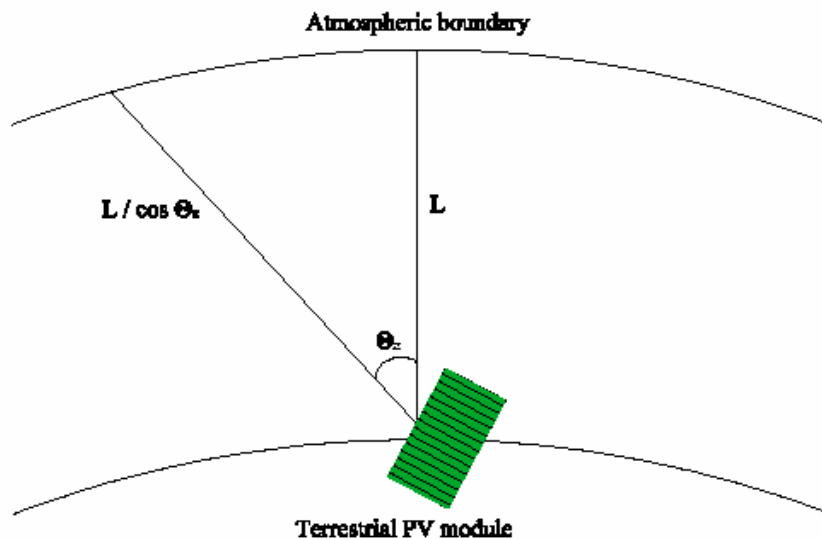


Figure 2.10 Diagram showing the inverse of the zenith angle cosine.

2.12.7 Photovoltaic cell material. The majority of photovoltaic cells are made from Silicon (Si), an inexpensive abundant material found in sand and other minerals. Due to its chemical and electrical semiconductor properties, silicon and its oxide, silicon dioxide, (SiO_2) has been used extensively in PV manufacturing over the years [Case, 2003]. Several other materials are available such as Indium Phosphide (InP), Copper Indium Deselenide (CuInSe_2) and Cadmium Telluride (CdTe). Unfortunately, these are not as commercially viable and as popular as silicon [Mazer, 1997]. The pie chart in figure 2.10 gives the percentage market share of cells manufactured from each material in 1998.

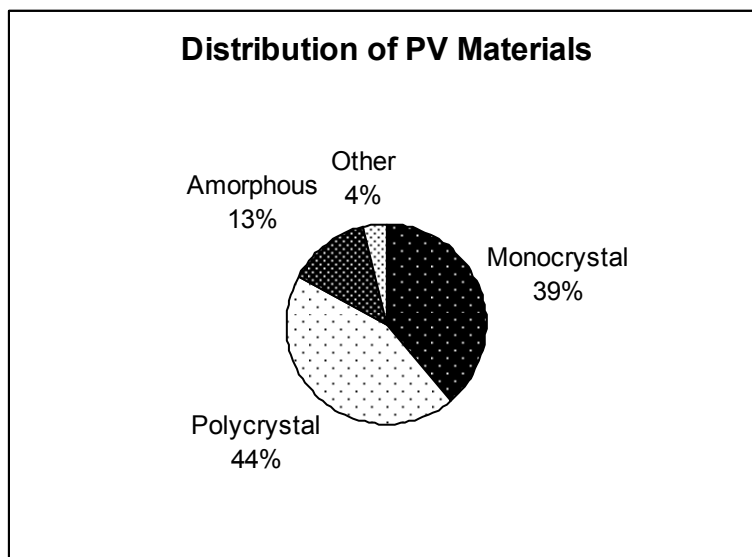


Figure 2.11 Market shares of photovoltaic materials [Markvart, 1998].

2.12.8 The silicon group. From Figure 2.11 it is evident that the majority of PV cells are manufactured from silicon. Within the silicon group there are three types of silicon used, the single or monocrystalline silicon, polycrystalline silicon and amorphous silicon. Crystalline silicon technology has evolved over the years as is evident in the milestone of a life span of 20 years or more and a production efficiency of about 18%. Amorphous silicon is less expensive and is usually used for solar powered watches and calculators [Markvart, 2000]. Polycrystalline silicon is used in an attempt to cut manufacturing cost although the finished product is not as efficient as monocrystalline silicon cells. Amorphous silicon which has no crystalline structure is

also used in an attempt to reduce production costs. Since these materials have different band gaps, they are tuned to different wavelengths or photons of different energies and hence have different conversion efficiencies [Aldous, 1998]. Table 2.1 gives a comparative range of cell efficiencies for three types of silicon materials.

Table 2.1 Conversion Efficiencies of Silicon Materials.

Material	Monosilicon	Polysilicon	Amorphous Silicon
Cell Efficiency (%)	15-18	12-13	3-7

2.13 Photovoltaic Energy Generating Systems

The use of photovoltaic cells as an energy production source is becoming more and more popular especially in developing countries. A full scale PV system is made up of several subsystems. Several cells in a series parallel combination are called a module or panel. Combining these module/panels in a further series combination is known as an array. To further boost the output of the system, solar tracker and concentrators are employed. A constant power source is assured with the addition of storage batteries and monitoring equipment such as inverters, voltage regulators, ammeters and voltmeters. Figure 2.11 shows a fully operational PV system.

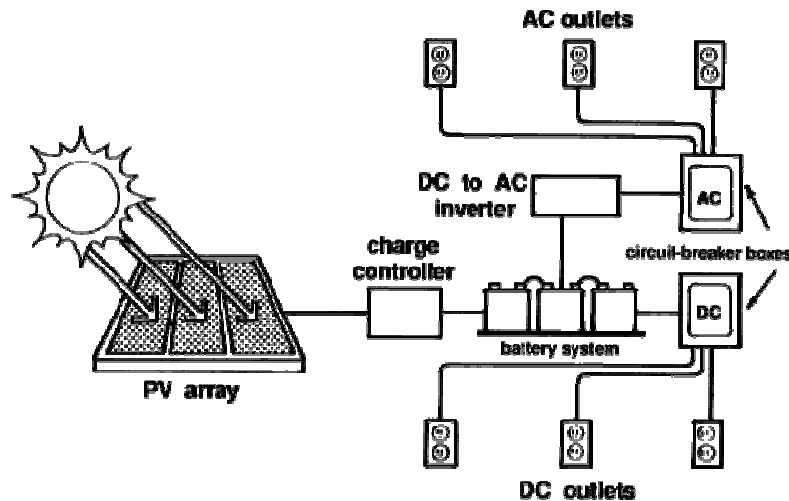


Figure 2.12 Complete PV System showing all internal and external components.

CHAPTER 3

METHODOLOGY

3.0 Introduction

One of the main objectives of this research was the design and fabrication of an automated solar tracking system. Critical to the research was the data collection. It was necessary to set up a framework from which to collect data. The project began with the sourcing of compatible components to build a solar tracking system. The system, which is passive in nature, required no motors or generators. The system was made up of three main components, the supporting structure, the moving parts and the solar modules.

3.1 Support Structure of the Solar Tracker

The primary supporting structure was made of reinforced concrete and was a three-foot tall, one-foot square pillar centered on a four-foot square base. Part of the supporting structure was an eighteen foot long hollow schedule forty structural rectangular steel beam affixed at the northern face of the concrete pillar as seen in Figure 3.1. The moving parts of the tracking system were the bidirectional winch, the cable pulley and the mounting pole. The bidirectional winch was employed to facilitate the raising and lowering of the solar modular mounting pole for the purpose of interchanging the solar modules. The pulley provides the mechanical advantage in raising and lowering the mounting pole.

The solar module simply sits upon the twenty-two foot tall aluminum pole inclined at an angle of 40 degree to the south as stipulated by equation: (3.1).

Angle of Inclination = Latitude – 15°, during the summer or Latitude + 15°, during the winter. The city of Tallahassee sits along the panhandle of Florida along latitude 24.5° N. The angle of inclination is calculated using equation (3.1).

$$\text{Angle of inclination} = 24.5^\circ + 15^\circ = 39.5^\circ \sim 40^\circ \quad 3.1$$

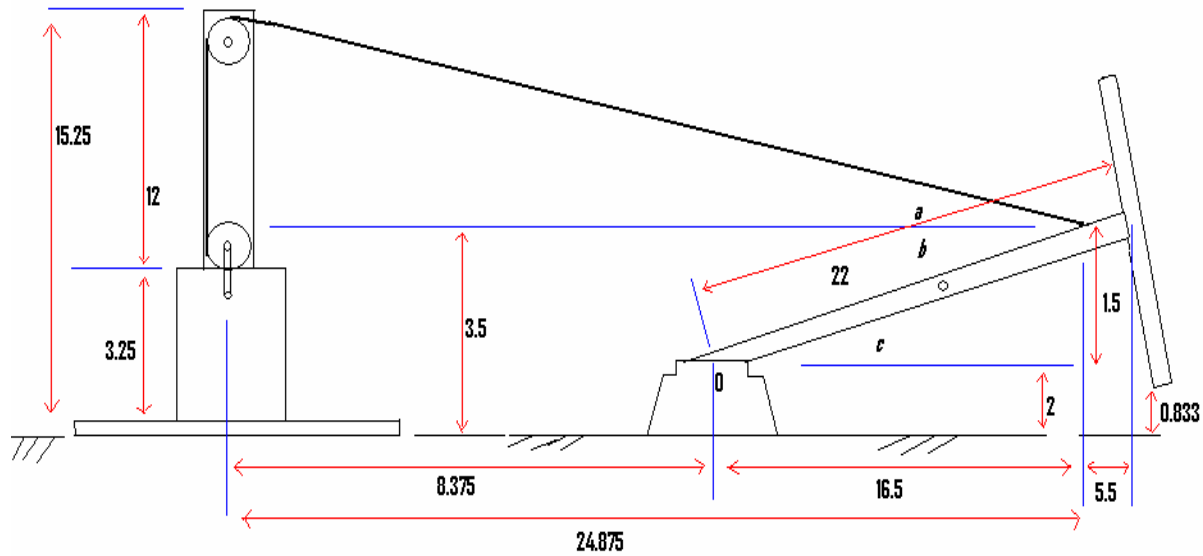


Figure 3.1 Drawing of the tracking system showing dimensions in feet of the winch assembly and support mechanism.

3.1.1 Design and fabrication of the tracking system. The system was designed around several parameters. Some of these parameters included the height and strength of the people who might operate the system, the weight of the many components, the materials used and the exposure to the elements as the system was located outdoors.

The most important operation of the system will be the raising and lowering of the solar panels. This process involves tensions in various directions. As a result, it was necessary to solicit an expert for assistance in determining the loads to be exerted on the various portions of the system [Moore, 2006]. The load values were then used to determine the strength and types of materials, angles and minimum distances for efficient operations.

The design process began with the calculation of the loads that the system would hold and the weight of the several moving parts of the system. Equations 3.2 through 3.5 shows the calculations derived before determining loads.

$$\text{Weight Module 1, } W_{m1} = 26 \text{ lbs} \quad 3.2$$

$$\text{Weight Module 1, } W_{m2} = 63 \text{ lbs} \quad 3.3$$

$$\text{Weight of tracking unit, } W_{tu} = 90 \text{ lbs} \quad 3.4$$

$$\text{Weight of Aluminum Pole } W_p = 3.46 \text{ lb/ foot} * 20 \text{ Feet} = 69.2 \approx 70.0 \text{ lbs} \quad 3.5$$

Hence maximum weight to be lifted by winch is approximately 179 lbs.

This information was then used to purchase a winch which had the capacity to lift a minimum load of 179 lbs. The gear ratio of this particular winch was 17.5:1. This simply means that for every 17.5 rotations of the winch handle, one (1) revolution of the winch drum is completed. In this case, the speed of moving the load is sacrificed for the ease at which the load is moved by the user. Also, integral in the choice of winch was the cable, its length and its material properties, particularly its breaking strain. Given a minimum requirement of 179 lbs, a 150 ft length of 5/16 twisted steel cable was chosen. Next, attention was turned to the mechanical advantage that could be offered to the winch by employing a pulley. Once the size of the cable was known, it was a simple matter of choosing a pulley with a minimum groove diameter of 5/16 of an inch.

From Figure 3.1, the total cable length was calculated using equation 3.6.

$$\begin{aligned} & 12 + \sqrt{15^2 + 24.875^2} \\ & 12 + \sqrt{843.77} \\ & = 42 \\ & \approx 50' \end{aligned} \quad 3.6$$

Next, using the dimensions of the bigger photovoltaic module, the maximum distance of the module off the ground that would allow a person of average height to perform maintenance on the tracking system was found to be ten (10) inches. The angles *a* and *b* were calculated to determine the position the cable should be affixed to the supporting pole in order to distribute the x and y forces on the pole when it is fully extended. Those calculations are shown in equations 3.7 and 3.8.

$$\begin{aligned} a &= \text{Tan}^{-1}(12 / 24.875) \\ &= 25.75^\circ \end{aligned} \quad 3.7$$

$$\begin{aligned} b &= \text{Tan}^{-1}(1.5 / 16.5) \\ &= 5.6^\circ \end{aligned} \quad 3.8$$

The addition of angles *a* and *b* gives an approximate angle of 30 degrees. This value will be used in the future to determine the force required to the pole and PV module to its vertical position.

Attention was then turned to calculation of the vertical force exerted on the cable when the module and pole are fully extended to their position ten (10) inches above the ground. A summation of the moment taken in the negative *y* or clockwise direction, which is equivalent to the vertical force taken from the point of rotation of the pole, is depicted by “O” in figure 3.5. The calculations for these forces are shown in equation 3.9.

$$\sum_{cw} = (11 * 70) + (22 * 70) = 2310 \text{ ftlbs} \quad 3.9$$

The value in equation 3.8 was then used to calculate the force in the upward force be exerted by the mechanical winch. This calculation is shown in equation 3.10.

$$\begin{aligned} 16.5x &= 70(11 + 22) \\ 16.5x &= 2310 \\ x &= 2310 / 16.5 \\ &= 140 \approx 150 \text{ ftlbs} \end{aligned} \quad 3.10$$

The reason for rounding up the calculated value to 150ftlbs was to increase the margin of safety. Using the results of equation 3.9 before rounding up, the force exerted on the winch, designated *x*, was calculated and is expressed in equation 3.11.

$$x = 140 * 16.5 = 2310 \text{ ftlbs} \quad 3.11$$

Equating equations 3.8 and 3.10 verifies that the system is balanced. Applying the result of equation 3.9 to determine the force, designated (*u f*), the user needs to apply to the winch system was calculated and shown in equation 3.12. where *n* is the mechanical advantage as given by the manufacturers of the winch.

$$\begin{aligned}
 Uf &= \frac{150}{n \sin \theta} \\
 &= \frac{150}{22 \sin 30^\circ} \\
 &= 13.63 \text{ lbs}
 \end{aligned}
 \tag{3.12}$$

Figure 3.2 shows a photo of the complete assembly of the solar tracking system designed and constructed for this research.

With all the major parts of the system chosen, attention was turned to calculating the loads that will be exerted on the assembled system. As seen in Figure 3.2, the solar module support pole was welded to a hinged two foot tall aluminum base that allows it to pivot in order to change the solar modules.

3.1.2 The tracking system. The tracking system was chosen based on its ability to make the entire system as autonomous as possible. The Zomeworks UTR020 Universal Track Rack allows for passive tracking of the sun throughout the day while gathering data and requiring limited maintenance.

3.1.3 Operation of the track rack. The “Track Rack” begins the day facing west. As the sun rises in the east, it heats the unshaded west-side canister, forcing liquid into the shaded east-side canister. As liquid moves through a copper tube to the east-side canister, the tracker rotates so that it faces east. The heating of the liquid is controlled by the aluminum shadow plates. When one canister is exposed to the sun more than the other, its vapor pressure increases, forcing liquid to the cooler shaded side. The shifting weight of the liquid causes the rack to rotate until the canisters are equally shaded. The movement of the tracking is schematically shown in Figure 3.3 [Zomeworks Corporation, 2000].



Figure 3.2 Photo of Completely Assembled Tracking System for the Research located at the Centennial building Innovation Park, Tallahassee.

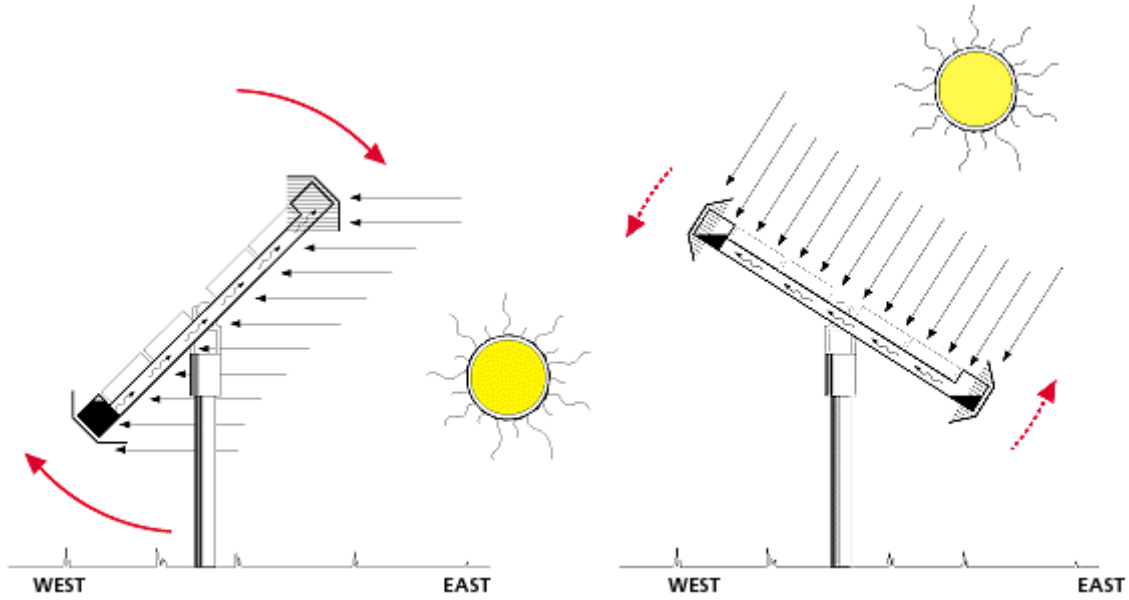


Figure 3.3a Tracking movement from east to west [Zomeworks Corporation, 2000]

As the sun moves, the rack follows continually (at approximately 15 degrees per hour) seeking equilibrium as liquid moves from one side of the tracker to the other. The rack completes its daily cycle facing west. It remains in this position overnight until it is "awakened" by the rising sun the following morning.

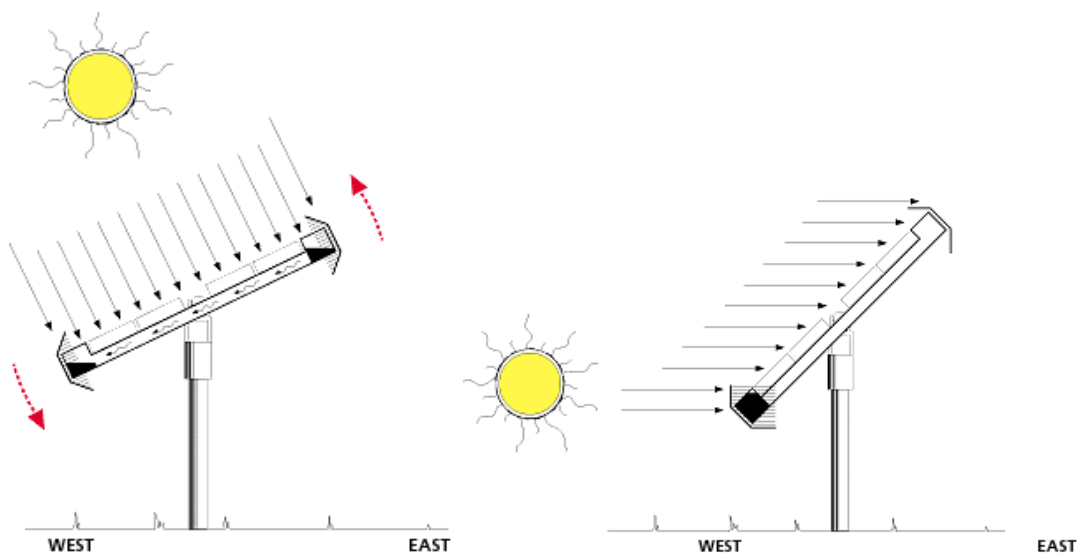


Figure 3.3b Tracking movement from east to west [Zomeworks Corporation, 2000].

3.2 Preliminary Data Analysis

The analysis was conducted at two levels: data collection was done first followed by statistical analysis using statistical tools and software. These statistical tools included Multiple Linear Regression (MLR), Random Complete Block Design (RBCD) and Design Expert software for generating an experimental design matrix. The experiment was designed to be conducted in three phases. The first phase was the verification of manufacturer specifications. The second phase was exposure of the two different panels to solar irradiance over a three day period in the month of March collecting energy output data and all relevant meteorological data every 5 minutes between the hours of 8 A.M. (0800 hrs) and 8 P.M. (2000 hrs). After two days, the positions of the panels were reversed and additional data collected for a further two days. The third phase was a repeat of the second phase with an exchange in the position of the panels and a change in the time of year to the month of May.

3.2.1 Types of data collection. Critical to the experimental process is the data collection. Data were collected in three basic forms. Historical data are the data collected by researcher in an area similar to that being studied and can be used as a basis for determining the validity of the data that were collected. Another type of data is experimental data. This is the data collected for the expressed purpose of determining the thesis objective. Finally, observational data which is data observed throughout the course of the data collection such as climatic conditions. The main data acquisition tool used in this thesis was a designed experiment.

3.2.2 Designed experiment. With a designed experiment being chosen as the procedure by which to conduct the analysis, the key elements were gathered and are listed in table 3.1.

3.2.3 The controllable factors. Four sets of controllable factors were considered. Data were collected for the entire daylight hours. However, emphasis was paid to the 10 am (1000 hrs) and 2pm (1400 hrs). The second factor was the tracking or non tracking mode. Two modes of data collection were employed, tracking using the solar tracking system and stationary. Next was material type. The two types crystalline modules studied were monocrystalline and polycrystalline. The last factor was the angle of inclination of the modules at an angle of zero degree (horizontal) and an angle of forty degrees.

Table 3.1 Choice of Factors and Levels for Design of Experiment

Choice of Factors and Levels		
	Factors	Levels
1	Tracking or Non Tracking	Yes , No
2	Time of Day	10a.m., 2p.m
3	Type of Material	Monocrystalline, Polycrystalline
4	Angle of Inclination	0 Degrees, 40Degrees

The experiment was carried out using the above mentioned six (6) factors. These factors were assigned various levels. Temperature was assigned two levels high and low, 20 degrees and 35 respectively. Time of day was assigned two levels of A.M. and P.M. The two levels assigned time of year were spring and summer while type of material was assigned the levels of monocrystalline and polycrystalline. Finally, Angle of inclination was assigned the two levels of inclined (40°) and flat (180°).

3.2.4 Nuisance factors. These factors as the name indicates can be an impediment to the production of electrical power. Cloud cover impacts the quality and quantity of solar irradiance incident on the solar modules. Precipital water vapor also called turbidity also affects the amount of solar irradiance reaching the module. Pollen count at certain times of the year can leave a film enough to severely impact the energy conversion process. During those times of year as a precautionary measure, the modules must be cleaned at least once per day.

The nuisance factors mentioned above invariably have an effect on the output power of the solar modules. However, for the purpose of this thesis, they will be considered as constants even though it creates a condition which subjects the solar modules to a film of pollen as thick as two to three millimeters and is liable to cause increased surface temperature of the module. Literature reviews suggest that, temperature probably causes the greatest reduction in energy output due to the material properties and its response increased temperature.

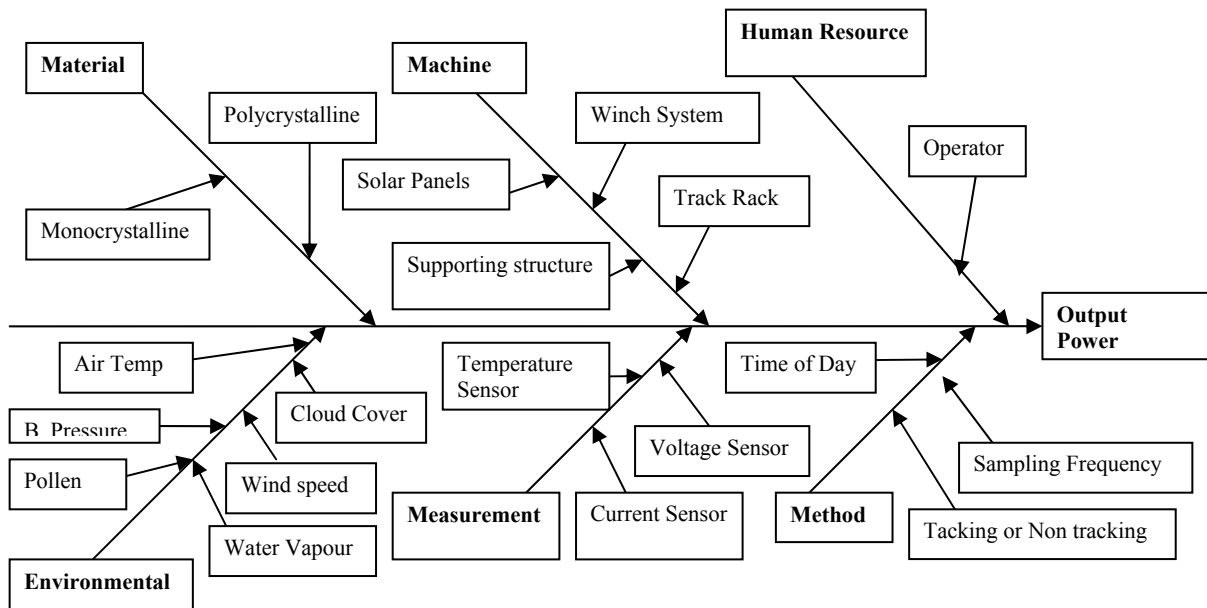


Figure 3.4 Fishbone diagram of factors affecting the power output of solar modules.

3.2.5 Response variable. Ultimately, the quantity of interest throughout this thesis is the output power measured in watts. This power is a function of voltage and current that was collected during the experimentation phase. These quantities are dealt with in more detail the “performing the experiment” section of this thesis.

3.2.6 Experiment Setup and Choice of Experimental Design:

The objectives of the thesis were four-fold:

1. To design and build a solar tracking system.
2. To determine through data collection using a data logger and several sensors the output of photovoltaic modules by tracking the trajectory of the sun as opposed to stationary arrangements.
3. To test monocrystalline and polycrystalline using the tracking system to determine the percentage increase in output of the modules as a result of tracking.
4. To verify whether the output of tracking system generates a maximum 30% increase in output when tracking is employed compared with stationary system.

The testing will be carried out considering that most solar testing is done under standard testing conditions which include a solar irradiance of 1000 W/m^2 , spectral distribution of 1.5 AM and at temperatures between of 25°C (77°F) and 45°C (113°F).

One of the main objectives of this thesis was the design and fabrication of an automated solar tracking system. Critical to the thesis was the data collection. It was necessary to set up a framework from which data could be collected. The project began with the sourcing of compatible components to build a solar tracking system. The system, which is passive in nature, required no motors or generators. It is comprised of three main components, the supporting structure, the moving parts and the solar modules.

The primary supporting structure is made of reinforced concrete and is a three-foot tall, one-foot square pillar centered on a four-foot square base. Also part of the supporting structure is a three-inch by six inch by eighteen feet long hollow structural rectangular steel affixed at the northern face of the concrete pillar as seen in Figure 3.1. The moving parts of the tracking system are the bidirectional winch, the cable pulley and the mounting pole. The bidirectional winch was employed to facilitate the raising and lowering of the solar module mounting pole for the purpose of interchanging the solar modules. The pulley provides the mechanical advantage in raising and lowering the mounting pole.

The solar module simply sits upon the twenty-two foot tall aluminum pole inclined at an angle of 40° to the south as stipulated by equation 3.1.

CHAPTER IV

DATA COLLECTION, ANALYSIS AND DISCUSSION

4.0 The Actual Experiment

A 2^4 factorial design with one replicate was chosen in order to adequately represent the conditions pertinent to the experiment. Originally, it was intended to have five factors. However, each factor that was added tended to be an environmental factor and could not be controlled and would cause an unnecessary level of difficulty. After consultation with an expert in design of experiments, the decision was made to reduce the number of factors to four and concentrate on the contribution that those factors would make the model.

Performing the Experiment: On the recommendation of a statistician, the experiment was performed in two parts in order to cover all possible combinations that might be germane to the data collection process. As a result, the monocrystalline and polycrystalline panels were interchanged on the solar tracker in two day intervals; simultaneously data was on the stationary panels at an angle of zero degrees. The same process was employed for the stationary panels at an angle of forty degrees. This is depicted in figure 4a, 4b and 4c. The question of whether to add center points or not arose and the decision not to add center points were based on the fact that adding center points to a 2^k design is based on the assumption that k factors are quantitative. The factors used in this thesis were a mixture of qualitative and quantitative factors which served as the basis for the exclusion of the center points. Also of interest was the decision to run a full factorial verses a fractional factorial. Using four factors (2^4 design) with a resolution of four (IV) or greater resulted in sixteen runs producing the finest results possible. A fractional factorial would have been unnecessary as time, resources and cost permitted the analysis of sixteen runs throughout the experimental process.

4.1 Data Collection

The data were collected using a configuration as shown in Figures 3.5 a, b and c respectively. To increase the ease with which the data were collected, a four channel data logger was employed. The logger is capable of sampling at several different rates. For the purpose of this project, only voltage, current and temperature were collected.



Figure 4.1a Data Collection Using Solar Tracker.



Figure 4.1b Data Collection in a Horizontal Configuration.



Figure 4.1c Data Collection Inclined at an Angle of Forty Degrees.

4.2 Data Analysis

The six step approach was chosen as a guide to perform the statistical analysis. The first step was to estimate the factor effects and examine their signs and magnitudes. This reveals preliminary information regarding which factors and interactions maybe important, and in which direction these factors should be adjusted to improve the response. In the third step, analysis of variance is used to test for significance of main effects and interaction. In step four, refining the model; usually consist of removing any nonsignificant variables from the full model. Step five is usual residual analysis to check for model adequacy and finally, graphical analysis – either main effects of interaction plots [Montgomery, 2005].

By using Design Expert software version 6.0, the data were analyzed with a view to determining the most influential factor or factors to the power (response variable). Review of the half normal plot shown in figure 4.2 revealed that Factor C (Material Type) was significant to the model. Studying the ANOVA table showed that not only was Factor C (Material Type) significant, but the lack of fit was also significant to the model as seen in table 4.1. A look at the R-squared and adjusted R-squared values (69.7% and 68.03%) respectively were indicators that a different model could indeed explain more of the variability associated with the analysis.

DESIGN-EXPERT Plot
Power

A: Tracking
B: Time of Day
C: Material Type
D: Inclined Angle

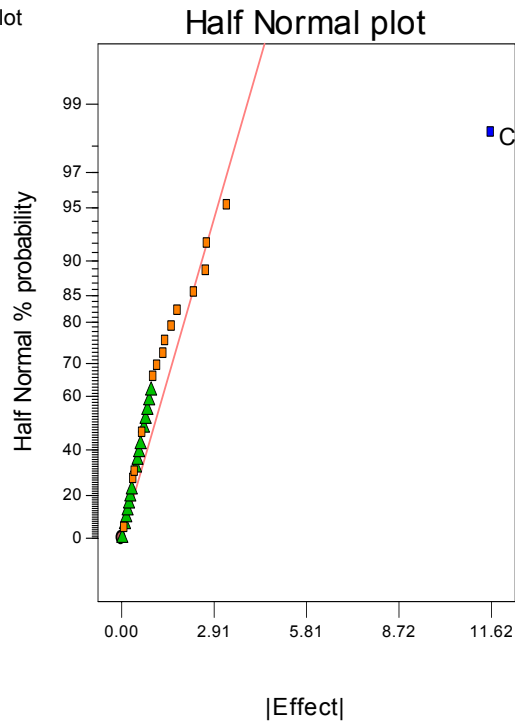


Figure 4.2 Half Normal Plot of Residuals.

Table 4.1 ANOVA Table from Initial Data Analysis

Analysis of variance table [Partial sum of squares]						
Source	Sum of Squares	DF	Mean Square	F Value	Prob > F	
Model	1080.9	1	1080.9	66.9784	< 0.0001	significant
C	1080.9	1	1080.9	66.9784	< 0.0001	
Residual	484.142	30	16.1381			
Lack of Fit	346.223	14	24.7302	2.86895	0.0231	significant
Pure Error	137.919	16	8.61996			
Cor Total	1565.04	31				

Consequently the analysis was rerun with additional factors chosen to decrease lack of fit and increase the R-squared values. The additional factors chosen were A (Tracking), B (Time of Day) and C (Material Type) with two two-factor interaction AC and BC as depicted in figure 4.3. Factors A and C are significant, however, factor B was not. Factor B was included in the model to preserve hierarchy. Factor interaction AC and BC are also significant and will assist in decreasing the lack of fit status.

Factor C was recognized to be a leading factor in terms of its significance to the response variable. In the first model with only factor C, it made sense that the material type plays a pivotal role in the power output of either solar panel. During the second analysis, it was evident that factors A, B and the 2FI's help to positively impact the model. Lack of fit was reduced to a level where it was no longer significant and the amount of variability explained by the model increased by approximately 10% as taken from the new ANOVA table, table 4.2. It stands to reason that factor A would be significant because the tracker is oriented so as to follow the trajectory of the sun and have maximum exposure to incident rays in the process which should increase output power.

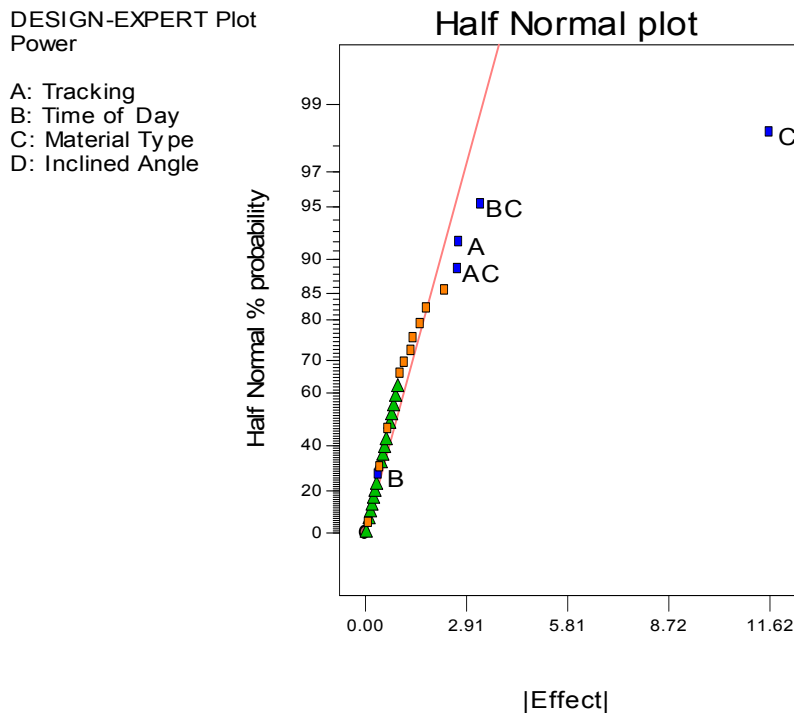


Figure 4.3 Second Generation Half Normal Plot of Data.

Table 4.2 Second Generation ANOVA Table

Analysis of variance table [Partial sum of squares]						
Source	Sum of Squares	DF	Mean Square	F Value	Prob > F	
Model	1286.154595	5	257.2309191	23.98084405	< 0.0001	significant
A	58.3740125	1	58.3740125	5.44202888	0.0277	
B	1.21119048	1	1.21119048	0.112915547	0.7395	
C	1080.901812	1	1080.901812	100.7691372	< 0.0001	
AC	56.8711125	1	56.8711125	5.301918155	0.0296	
BC	88.79646848	1	88.79646848	8.278220482	0.0079	
Residual	278.8894287	26	10.72651649			
Lack of Fit	140.9701293	10	14.09701293	1.635392638	0.1834	not significant
Pure Error	137.9192994	16	8.619956211			
Cor Total	1565.044024	31				

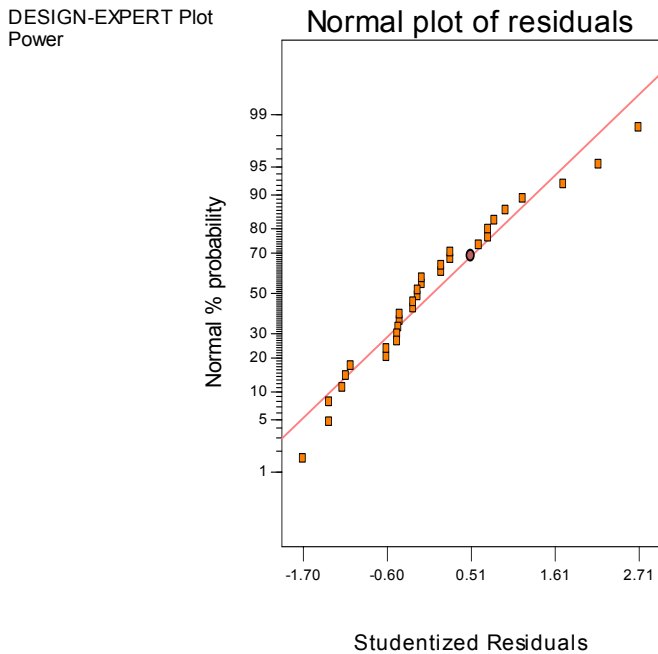


Figure 4.4 Second Generation Normal Plot of Residuals.

The normal plot of residuals is a graphical representation of the assumption that the data are normally distributed. An indication of normality is the data are plotted against a theoretical normal distribution in such a way that the points should form an approximate straight line. Departures from this straight line indicate departures from normality.

A plot of residuals against the value of a fitted response should yield a distribution of points scattered randomly about 0, irrespective of the size of the fitted value. More often than not, residual values may increase as the corresponding fitted value increases. When this occurs, the residual pattern becomes "funnel shaped" with the larger end toward larger fitted values; that is, the residuals have larger and larger scatter as the value of the response values increases. As it applies to this data as shown in figures 4.5a through figures 4.5e, no abnormalities are detected suggesting the data are uniformly scattered and fall within the three standard deviations.

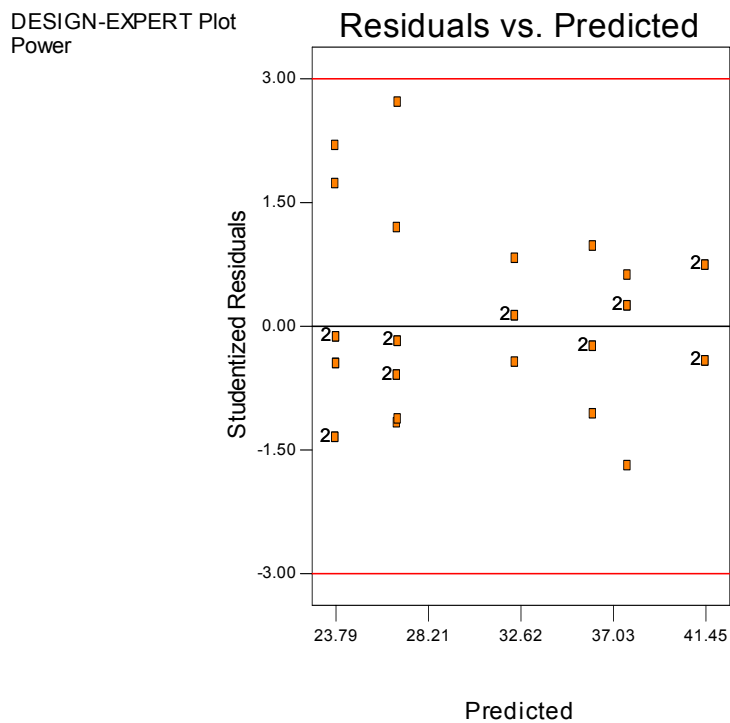


Figure 4.5a Plot of Residuals vs. Predicted Values.

DESIGN-EXPERT Plot
Power

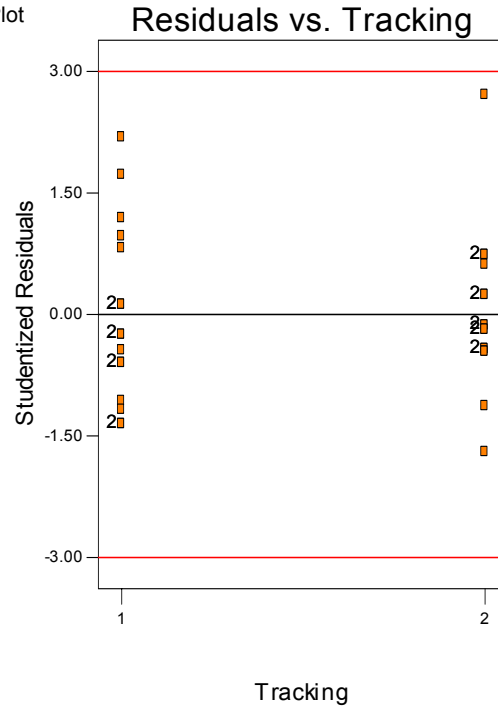
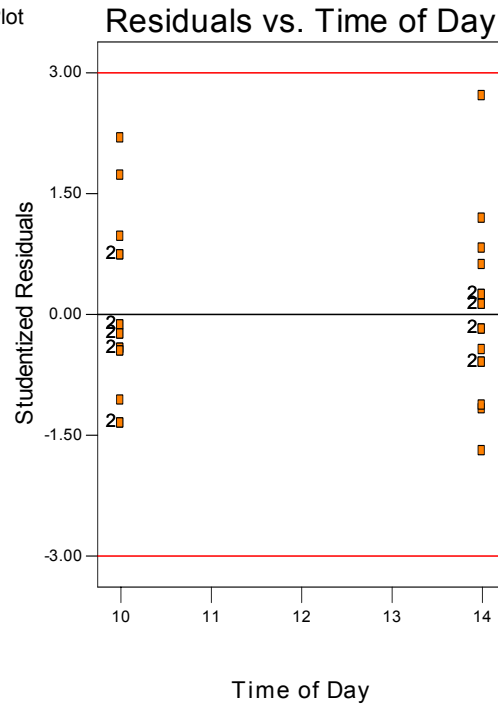


Figure 4.5b Plot of Residuals vs. Tracking.

DESIGN-EXPERT Plot
Power



DESIGN-EXPERT Plot
Power

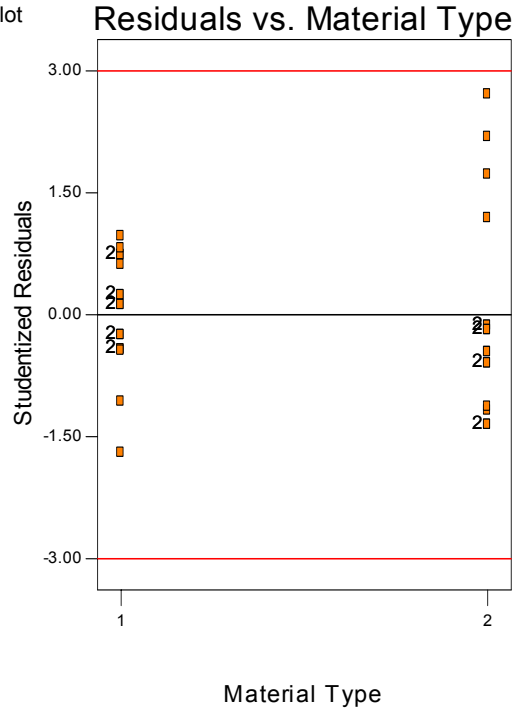


Figure 4.5d Plot of Residuals vs. Material Type.

DESIGN-EXPERT Plot
Power

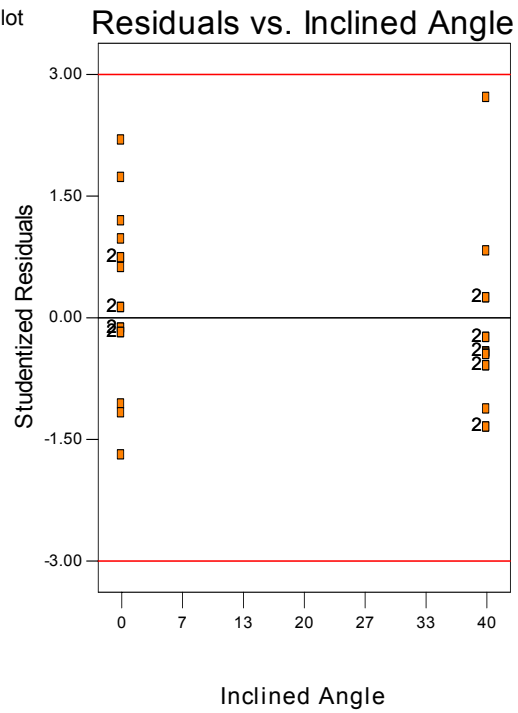


Figure 4.5e Plot of Residuals vs. Inclined Angle.

In support of figures 4.5a through 4.5e is the Box-Cox plot in figure 4.6 indicates that no transformation of the data is necessary.

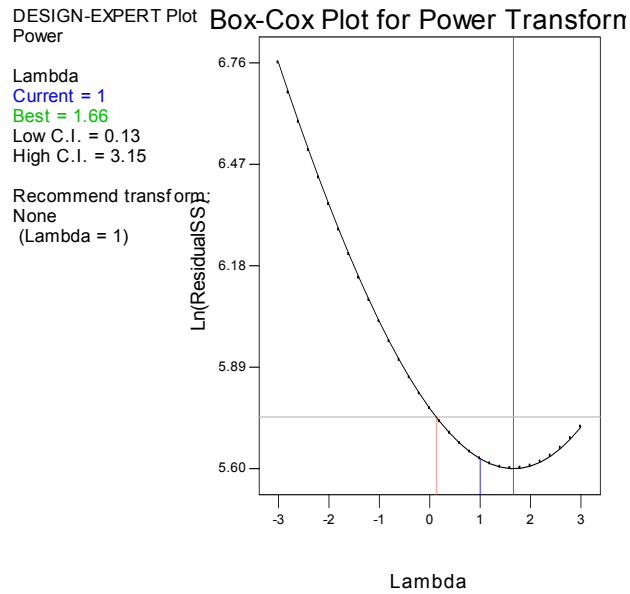


Figure 4.6 Plot of Box-Cox Transformation.

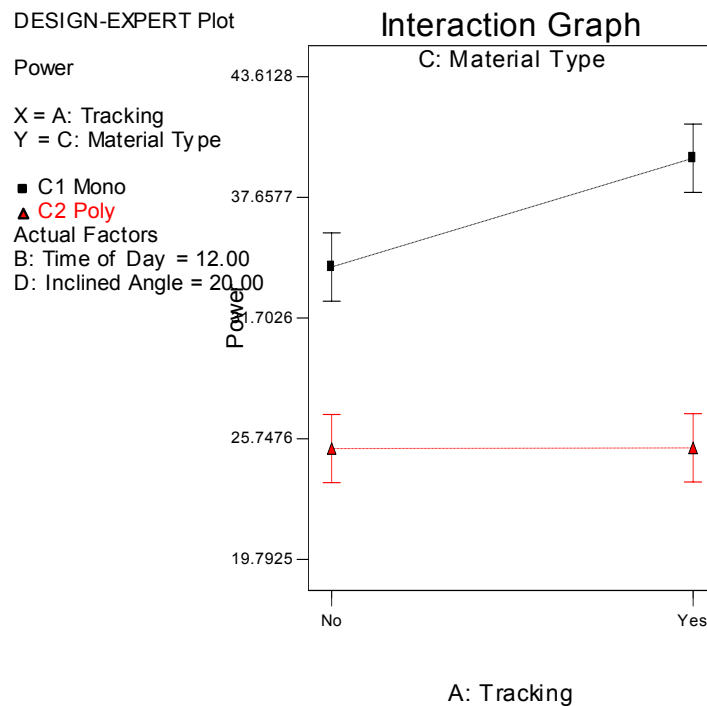


Figure 4.7 Interaction of Monocrystalline and Polycrystalline as a Function of Tracking.

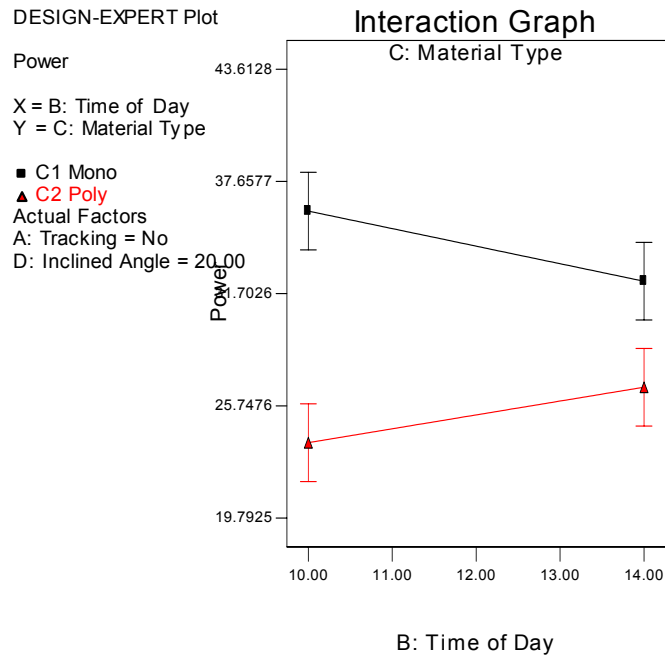


Figure 4.8 Interaction of Monocrystalline and Polycrystalline as a Function of Time of Day.

The interaction AC depicts how important trajectory and material type are for power output. It is surprising that factor B is not as significant as would be expected. The rationale behind this assertion is that solar incident rays are most intense when the sun is as close to its zenith through out the day. Figure 4.9 shows that for both stationary flat and concentrator (tracking) the maximum power at an hour plus and minus the midday hour with the concentrator having the greater power output over a greater time range.

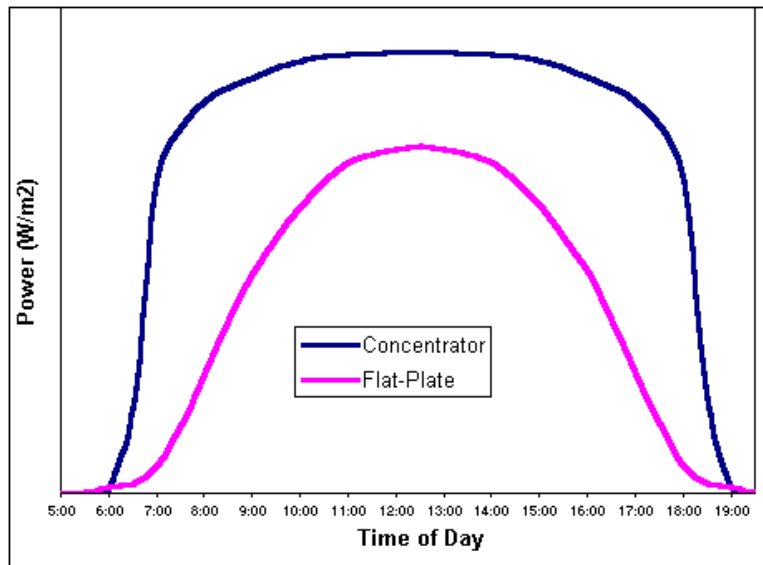


Figure 4.9 Difference of power between Flat and Tracking [NREL, 2001].

On the contrary, when factor B interacts with C, there is a significant change in the response model which speaks to the overwhelming effect that the material type has on the power output. The diagnostics of the data analysis indicates randomization, even distribution and no outliers among the data points. They also support the assumption of normality.

4.3 Refining the Model Equation

Before the model equation could be accepted, it was noticed that from the second generation of plots, particularly the Half Normal plot of main effects, there was another factor that could be included in the model building process. Experiments can contain qualitative as well as quantitative factors, both of which are treated identically in the analysis process. Only the differences between the levels of factors are of interest with the final product being an empirical model of the process that has been studied by developing an interpolation equation for the response variable in the equation [Montgomery, 2005].

As a result of the addition of another factor to the model, steps four through six of the six step approach to analysis were revisited. These are refining the model, analysis of the residuals and interpretation of the results.

With the addition of interaction of time-of-day and inclined angle, the single factor inclined angle was automatically added to the model to preserve hierarchy as shown in figure 4.10. Figures 4.11a through 4.11e are the corresponding diagnostic plots for the refined model.

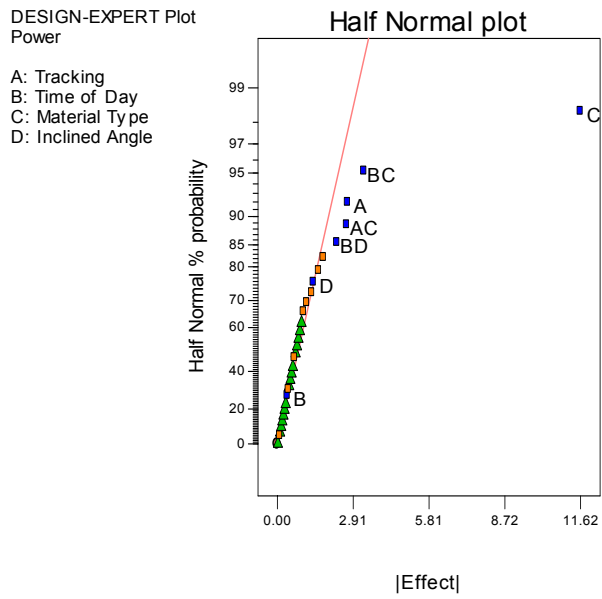


Figure 4.10 Refined Half Normal Plot of Main Effects.

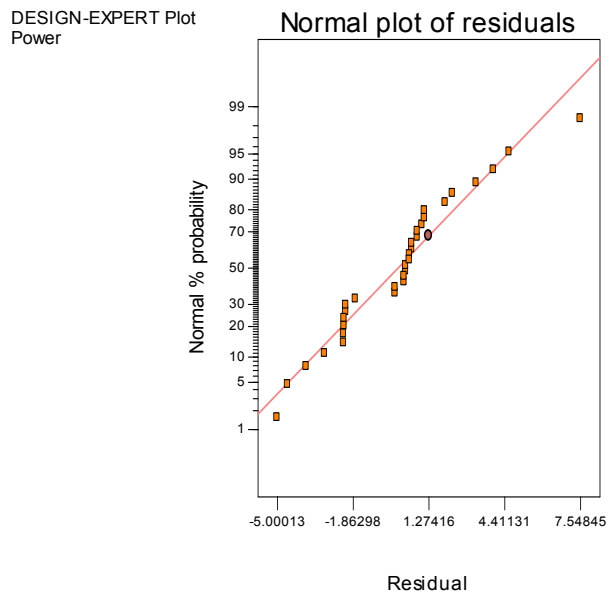


Figure 4.11 Third Generation Normal Probability Plot of Effects.

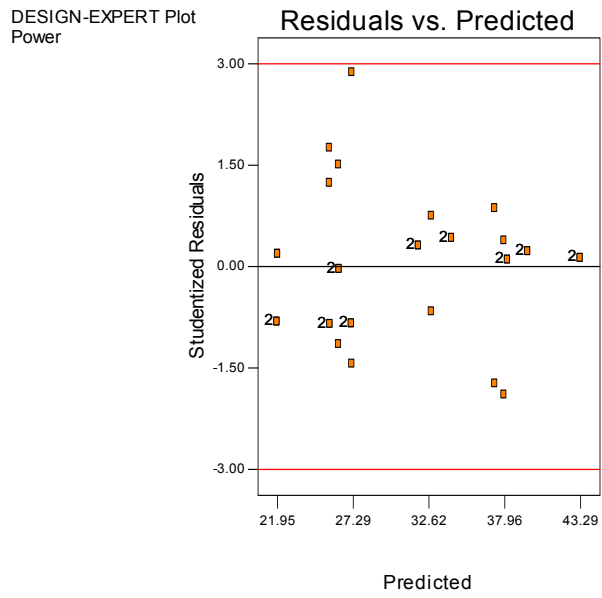


Figure 4.12a Third Generation Plot of Residuals vs. Predicted Values.

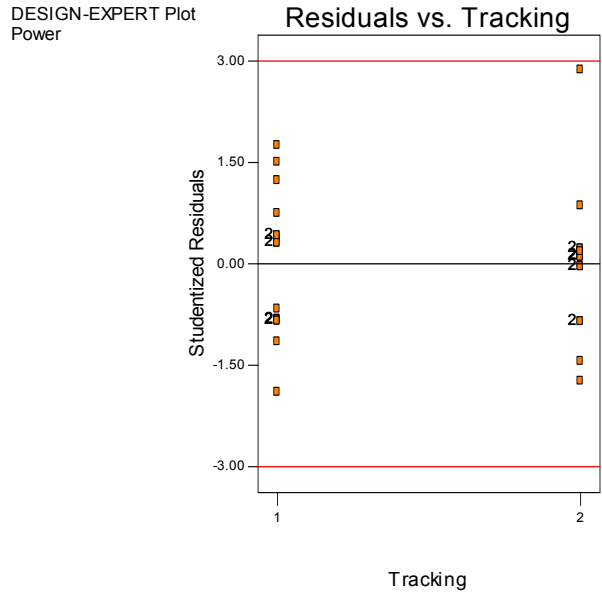


Figure 4.12b Third Generation Plot of Residuals vs. Tracking.

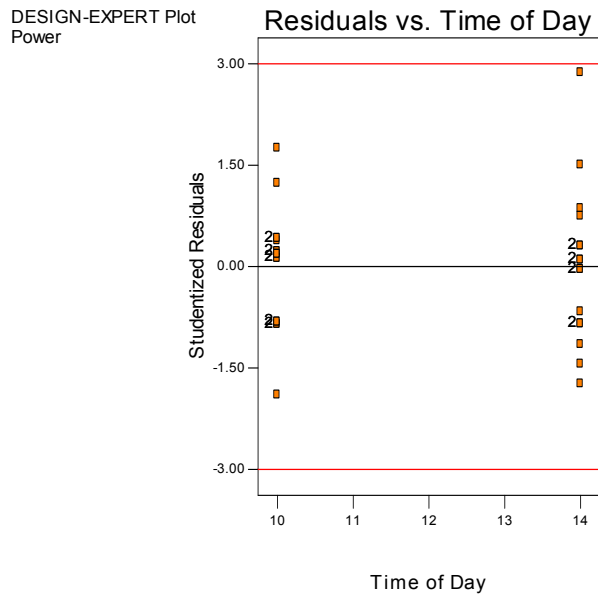


Figure 4.12c Third Generation Plot of Residuals vs. Time-of-Day.

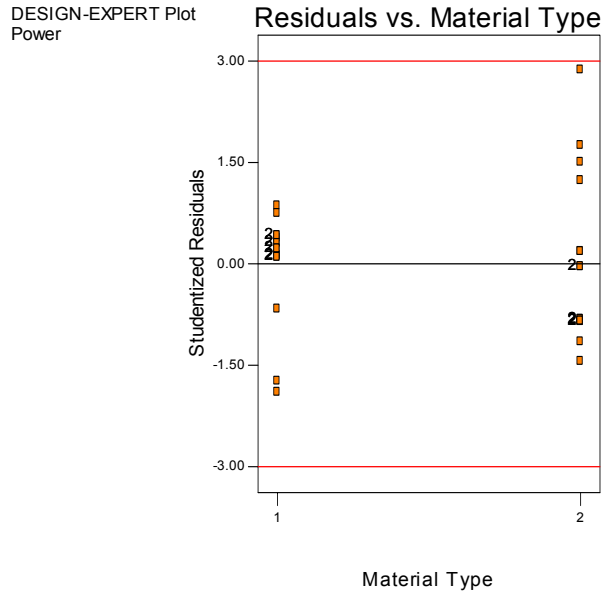


Figure 4.12d Third Generation Plot of Residuals vs. Material Type.

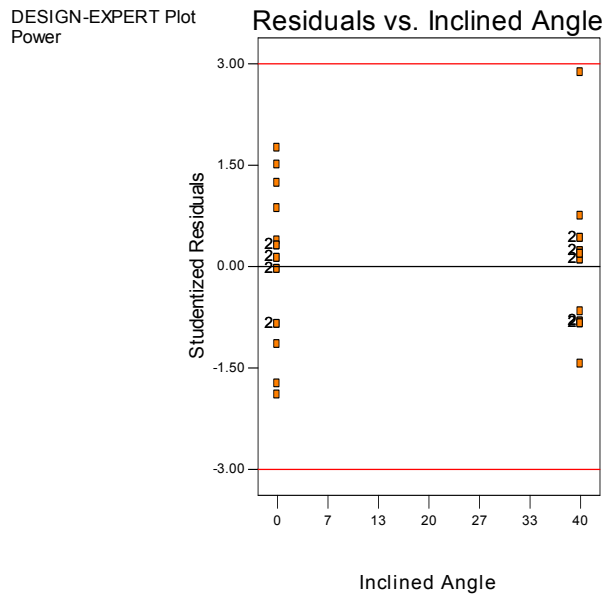


Figure 4.12e Third Generation Plot of Residuals vs. Inclined Angle.

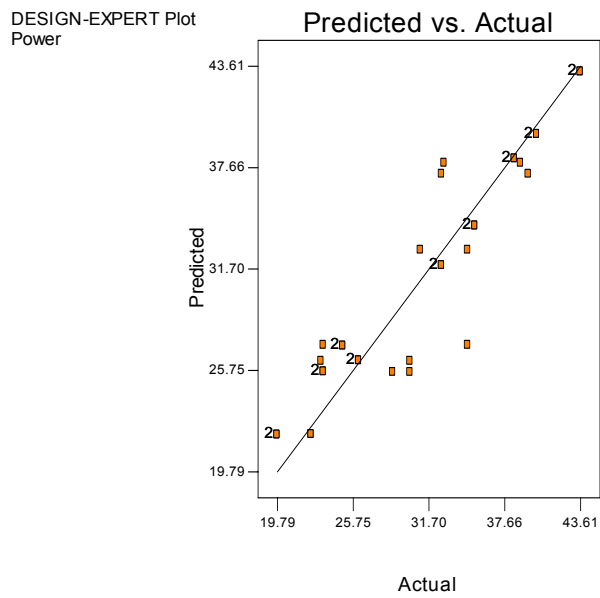


Figure 4.13 Third Generation Plot of Predicted vs. Actual Values.

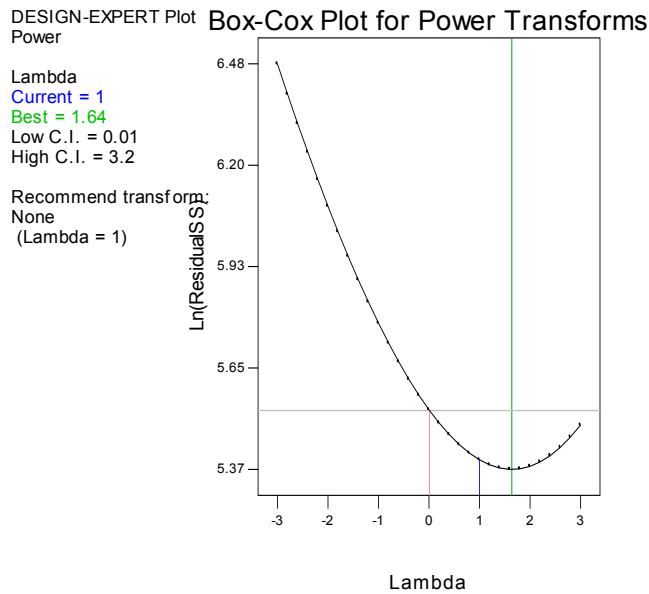


Figure 4.14 Third Generation Plot of Box-Cox Transformation.

4.4 Validation

The final step in any experiment is to predict the response at the optimal settings. Confirmation runs can then be done to verify your prediction. Point prediction allows you to enter levels for each factor or component into the current model. Design Expert then calculates the expected responses and associated confidence intervals based on the prediction equation that is shown in the ANOVA output. The predicted values are updated as the levels are changed.

The 95% CI (confidence interval) is the range in which you can expect the process average to fall into 95% of the time. The 95% PI (prediction interval) is the range in which you can expect any individual value to fall into 95% of the time. The prediction interval will be larger (a wider spread) than the confidence interval since you can expect more scatter in individual values than in averages. (Note that the % interval can be changed to 90%, 95% or 99% as desired. The optimization tool was used to compare the actual responses with the predicted model. In particular, the material type, the tracking and the angle were all varied and investigated at three different times within the experimental time interval. In all cases, the actual responses fell within both the confidence and predicted intervals. This is an indication that the model equation 4.1 is good for estimating the power output of either solar module.

Table 4.3 Sample of Generated Prediction Run

Factor	Name	Level	Low Level	High Level	Std. Dev.		
A	Tracking	Yes	No	Yes	N/A		
B	Time of Day	13	10	14	0		
C	Material Type	Poly	Mono	Poly	N/A		
D	Inclined Angle	40	0	40	0		
	Prediction	SE Mean	95% CI low	95% CI high	SE Pred	95% PI low	95% PI high
Power	26.034375	1.228176038	23.509823	28.558927	3.497847	18.8444477	33.22430225

$$\text{Power} = 31.09 + 1.35 * A - 0.19 * B - 5.81 * C - 0.70 * D - 1.33 * AC + 1.67 * BC + 1.15 * BD$$

4.1

The experimental results have shown that monocrystalline solar panels produce a greater power output than the polycrystalline panel. This is substantiated by the one factor and interaction plots associated with the data. It is clear that tracking does play an important role in the power output of the solar panels. In addition, the influence of the monocrystalline solar panel to the power output can be positively or negatively impacted depending on the factor with which it interacts. An example of this can be seen in the interactions between factors tracking and material type and time of day and the material type. Previous research has shown that monocrystalline panels have a higher power conversion rate than polycrystalline.

Having summarized that the monocrystalline PV module produces more power output than the polycrystalline, a final experiment was setup to determine the percentage difference in power output between three monocrystalline modules in zero degree, forty degree and tracking configuration. The three modules were set up to collect data over a five day period. A sample of the raw data is shown in table 4.4. From these data, MINITAB software was used to generate a

scatter plot of the data. The scatter plot can be seen in figure 4.15. The data was plotted without the aid of data transformation software. All three graphs are superimposed on each other to display their relative relationships to each other. From figure 4.15, the average power was calculated for the three main regions of the graph. These regions can be considered the linearly increasing, monotonic and linearly decreasing respectively.

Table 4.4 Sample raw data collected from 0 degree, 40 degree and tracker respectively

Date and Time	0 (W)	40 (W)	Trac (W)
8/26/06 8:30	14.4375	1.155	24.2064
8/26/06 8:35	16.185	1.2075	35.5152
8/26/06 8:40	18.69	1.2075	38.4336
8/26/06 8:45	20.445	1.5	38.6784
8/26/06 8:50	24	1.89	38.6784
8/26/06 8:55	25.9875	2.4	38.1888
8/26/06 9:00	27.795	2.97	36.96
8/26/06 9:05	30.24	4.515	31.5744
8/26/06 9:10	30.78	5.5125	36.72
8/26/06 9:15	31.32	7.56	35.7504
8/26/06 9:20	32.745	9.6	35.7504
8/26/06 9:25	33.0225	11.715	35.5152
8/26/06 9:30	34.2	14.8125	35.5152
8/26/06 9:35	34.2	17.82	35.5152
8/26/06 9:40	34.485	20.445	35.28
8/26/06 9:45	34.485	23.25	35.28
8/26/06 9:50	34.485	25.2	35.5152
8/26/06 9:55	34.485	26.73	35.28
8/26/06 10:00	34.485	29.1375	35.5152
8/26/06 10:05	34.485	29.6625	35.28
8/26/06 10:10	34.485	30.78	35.28

Table 4.4 Continued			
8/26/06 10:15	34.485	31.05	35.0448
8/26/06 10:20	34.485	31.59	35.28
8/26/06 10:25	34.485	31.86	35.28
8/26/06 10:30	35.3925	33.0225	33.8688

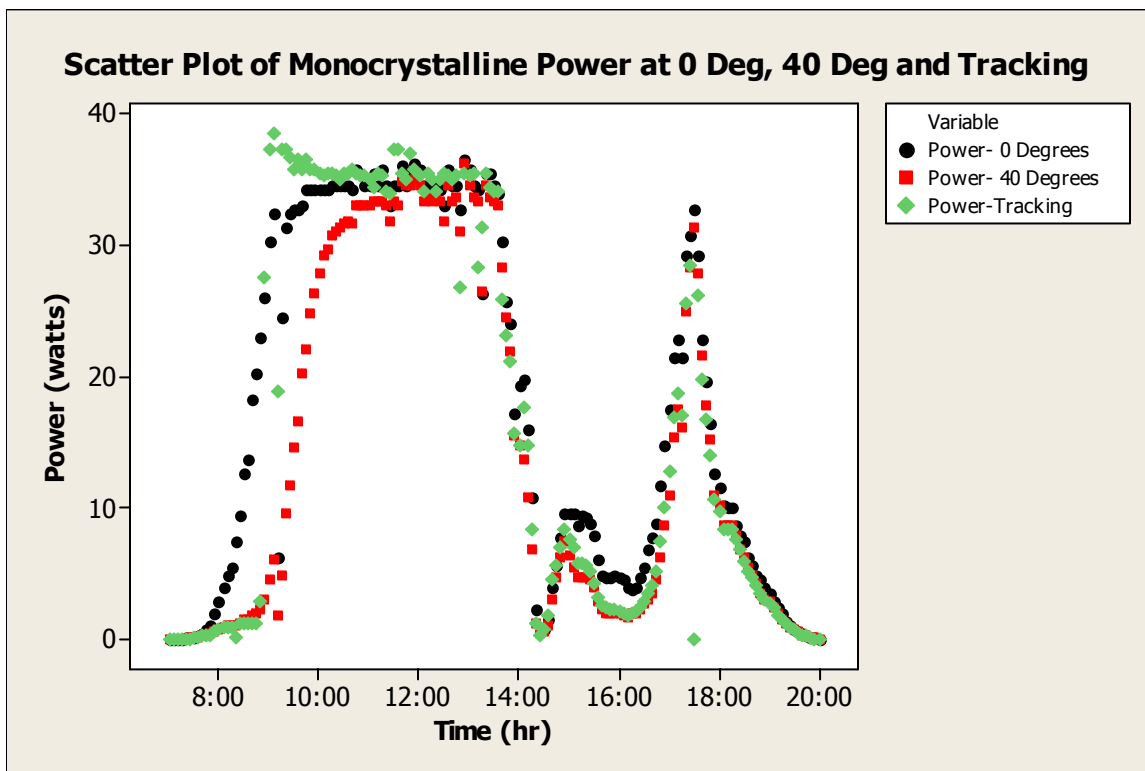


Figure 4.15 Scatter Plot of Monocrystalline Power Generated at 0°, 40° and Tracking.

4.5 Confirmation

Using Microsoft Excel, the average power was calculated for these three regions. For the linearly increasing region, the period chosen was between 08:30 and 10:00. For the monotonic region the period chosen was between 10:00 and 14:30 and for the linearly decreasing region, the

period chosen was between 17:30 and 19:30. However, because linear increasing and linear decreasing regions were outside the scope of this thesis, the period between 10:00 and 14:30 was concentrated on. Times were chosen at thirty minute intervals and the percentage power difference between 0 degrees and tracking and between 40 degrees and tracking was calculated. Table 4.5 shows these calculations and the final average power calculations.

Table 4.5 Power values of figure 4.15 and percentage difference between configurations

Date and Time	0 Deg	40 Deg	Tracking	% Pwr Difference Between Trac & 0	% Pwr Difference Between Trac & 40
8/26/06 10:00	34.4850	29.1375	35.5152	2.98738582	21.88828829
8/26/06 10:30	35.3925	33.0225	35.8688	1.345765346	8.619274737
8/26/06 11:00	34.4850	33.5775	35.9856	4.351457155	7.171766808
8/26/06 11:30	17.2125	11.8800	37.2000	116.1220044	213.1313131
8/26/06 12:00	19.7925	17.4150	32.2608	62.99507389	85.24720069
8/26/06 12:30	34.2000	33.3000	32.7120	-4.350877193	-1.765765766
8/26/06 13:00	26.2350	29.6625	40.1856	53.17552887	35.47610619
8/26/06 13:30	34.2000	34.7700	34.5600	1.052631579	-0.603968939
8/26/06 14:00	34.4850	33.5775	35.5152	2.98738582	5.77082868
8/26/06 14:30	35.6850	34.7700	35.9856	0.842370744	3.496117343
	Average Percent Difference			24.15%	37.84%

Table 4.5 displays the calculations based on the comparisons between the power output from tracking and zero degrees and tracking and forty degrees. Even with minor fluctuations in the power output due to climatic changes, the average power output was greater in favor of the tracking system. The average increase was calculated to be 24% and 37% over the zero and forty degree configuration respectively.

CHAPTER V

ANALYSIS, RESULTS AND CONCLUDING REMARKS

This research confirms that the interaction between tracking and the monocrystalline continues to produce higher power output than polycrystalline solar module, the results concur with those of previous researchers [Case, 2003]. Additionally, this power output is improved in tracking mode. Table 4.5 further supports this statement through percentages that indicate that the on the average, the power output through tracking exceeds that of flat modules by 24% and forty degree inclination by 37%. It would be remiss not to mention the fact that as seen through the analysis, several factors are brought to bear on the performance on the monocrystalline modules even though their power output in tracking mode exceed that of flat and 40 degree inclined.

Aside from the factors analyzed, other factors affecting the model and hence the ability to reasonably predict the power output are pollen count, humidity and barometric pressure. Additionally, a look at Figure 4.15 calls to mind the possible effect of temperature on the power output. Inspection of the behavior of the graph from approximately 14:00 hrs to 17:30hrs, known to be the hottest period of the day, suggest that temperature might have played a significant role in the power output. This may bear some credence especially since all three modules behaved in a similar manner in different configurations.

5.1 Recommendations and Future Work

- a) Throughout the analysis, several conclusions were drawn.
- b) The first indicates that the monocrystalline module is more favorable for power generation than the polycrystalline.
- c) It further concludes that tracking is the preferred method for garnishing this power.
- d) Hence it would stand to reason that monocrystalline modules should be recommended for private and commercial photovoltaic power generation needs.
- e) If tracking is to be chosen over stationary flat or inclined configuration, then a further recommendation is to employ a tracking system whether active or passive that faces east as early in the morning as possible and not one that uses first light to “wake up” and traverse to an easterly direction before power can be generated. This gives the advantage

of generation power as early as possible increasing the overall power generating capacity throughout the day.

- f) Another recommendation would be to recollect data paying close attention to the significance temperature has on the power production. Figure 4.15 depicts climatic anomaly around 2:30 pm (14:30 hrs) which affects the power output for several hours and suggest that temperature was a contributing factor.

Environmental factors that are thought to affect the power output were shading of the modules, high pollen count and cloud cover. Shading can be alleviated by ensuring man made objects are free and clear of the experimental setup. Pollen count can be avoided by choosing a season when pollen count is low. Cloud cover is simply uncontrollable. The results of this experiment indicate factors that can expand solar research. As the significant factors from this experiment are further explored, larger and broadly impacting conclusions can be drawn about solar modules and power output.

APPENDIX A

Energy Related Conversion Factors

1 Barrel = 42 Gallons = 159.0 Liters

1Btu = 252.0 Calories = 1055 joules

1000 Joules = 0.9479 Btu

1 Joule = 0.2388 Calories

1 Calorie = 4.187 Joules

1 Kilowatthour = 3.600×10^6 Joules = 3412 Btu

1 Watt = 1joule/second = 3412 Btu/hr

1 Btu/hr = 0.2931 Watts

APPENDIX B – EXPERIMENTAL DATA

Table D.1 Sample Experimental and Transformed Data

Date and Time	Scaled I	Scaled V	Scaled 3	Scaled 4
8/26/06 10:00	0.604	0.196	18.12	1.96
8/26/06 10:05	0.6	0.196	18	1.96
8/26/06 10:10	0.6	0.196	18	1.96
8/26/06 10:15	0.596	0.196	17.88	1.96
8/26/06 10:20	0.6	0.196	18	1.96
8/26/06 10:25	0.6	0.196	18	1.96
8/26/06 10:30	0.588	0.192	17.64	1.92
8/26/06 10:35	0.42	0.14	12.6	1.4
8/26/06 10:40	0.596	0.192	17.88	1.92
8/26/06 10:45	0.632	0.204	18.96	2.04
8/26/06 10:50	0.596	0.192	17.88	1.92
8/26/06 10:55	0.444	0.148	13.32	1.48
8/26/06 11:00	0.612	0.196	18.36	1.96
8/26/06 11:05	0.6	0.192	18	1.92
8/26/06 11:10	0.608	0.196	18.24	1.96
8/26/06 11:15	0.596	0.192	17.88	1.92
8/26/06 11:20	0.388	0.132	11.64	1.32
8/26/06 11:25	0.58	0.188	17.4	1.88
8/26/06 11:30	0.62	0.2	18.6	2
8/26/06 11:35	0.612	0.196	18.36	1.96
8/26/06 11:40	0.436	0.144	13.08	1.44
8/26/06 11:45	0.608	0.196	18.24	1.96
8/26/06 11:50	0.6	0.196	18	1.96
8/26/06 11:55	0.6	0.196	18	1.96
8/26/06 12:00	0.572	0.188	17.16	1.88
8/26/06 12:05	0.596	0.192	17.88	1.92
8/26/06 12:10	0.604	0.196	18.12	1.96
8/26/06 12:15	0.484	0.16	14.52	1.6
8/26/06 12:20	0.612	0.2	18.36	2

8/26/06 12:25	0.5	0.168	15	1.68
8/26/06 12:30	0.58	0.188	17.4	1.88
8/26/06 12:35	0.516	0.168	15.48	1.68
8/26/06 12:40	0.484	0.16	14.52	1.6
8/26/06 12:45	0.648	0.208	19.44	2.08
8/26/06 12:50	0.624	0.204	18.72	2.04
8/26/06 12:55	0.444	0.148	13.32	1.48
8/26/06 13:00	0.644	0.208	19.32	2.08
8/26/06 13:05	0.612	0.2	18.36	2
8/26/06 13:10	0.336	0.112	10.08	1.12
8/26/06 13:15	0.628	0.204	18.84	2.04
8/26/06 13:20	0.52	0.168	15.6	1.68
8/26/06 13:25	0.604	0	18.12	0
8/26/06 13:30	0.6	0.192	18	1.92

**Table D.2 Sample Experimental and Transformed Data
(Design Matrix)**

Std	Run	Block 1	Tracking	T of D	Material	Incline	Power
16	1	Block 1	Yes	14	Poly	0	26.208
5	2	Block 1	No	14	Mono	0	32.712
29	3	Block 1	No	14	Poly	40	24.96
19	4	Block 1	Yes	10	Mono	40	40.1856
14	5	Block 1	No	14	Poly	0	30.24
2	6	Block 1	No	10	Mono	0	32.9232
15	7	Block 1	Yes	14	Poly	0	26.208
1	8	Block 1	No	10	Mono	0	38.9232
3	9	Block 1	Yes	10	Mono	0	43.6128
12	10	Block 1	Yes	10	Poly	0	23.424
24	11	Block 1	Yes	14	Mono	40	38.4336
8	12	Block 1	Yes	14	Mono	0	39.5344
32	13	Block 1	Yes	14	Poly	40	23.424
17	14	Block 1	No	10	Mono	40	35.34
30	15	Block 1	No	14	Poly	40	24.96

Table D.2 Continued							
20	16	Block 1	Yes	10	Mono	40	40.1856
21	17	Block 1	No	14	Mono	40	34.77
27	18	Block 1	Yes	10	Poly	40	22.468
11	19	Block 1	Yes	10	Poly	0	23.424
10	20	Block 1	No	10	Poly	0	30.24
26	21	Block 1	No	10	Poly	40	19.7925
22	22	Block 1	No	14	Mono	40	31.05
31	23	Block 1	Yes	14	Poly	40	34.77
4	24	Block 1	Yes	10	Mono	0	43.6128
9	25	Block 1	No	10	Poly	0	28.875
7	26	Block 1	Yes	14	Mono	0	32.712
28	27	Block 1	Yes	10	Poly	40	22.464
23	28	Block 1	Yes	14	Mono	40	38.4336
13	29	Block 1	No	14	Poly	0	23.25
25	30	Block 1	No	10	Poly	40	19.7925
18	31	Block 1	No	10	Mono	40	35.34
6	32	Block 1	No	14	Mono	0	32.712

APPENDIX C – EXPERIMENTAL EQUIPMENT



30 Volted Sensor



10 Apm Current Sensor



10 Ohm, 220 Watt Load Resistor



Solar 1 4 Channel Data Logger

REFERENCES

- Berger, John J. Charging Ahead: The Business of Renewable Energy and What It Means for America. New York: Henry Holt and Company. 1997.
- Boyle, Godfrey, ed. Renewable Energy: Power for a Sustainable Future. UK: Oxford University Press. 1996.
- Carlsson, Thomas K.J., Experimental set up for full scale field test of CdTe and Cis thin film PV modules, November 2001
- Case, Michael O. Comparative Analysis for the Effects of Meteorological Parameters on the Output of Crystalline Silicon Photovoltaic Modules, Florida state University, 2003
- Department of Energy, Renewable Energy Annual 1997. Vol I. Washington, DC: 1997.
- Fukae et al. Outdoor performance of triple stacked A-Si photovoltaic modules in various geographical locations and climates. In *IEEE Photovoltaic*
- Fundamentals of Photovoltaic Materials, Olivia Mah NSPRI Report
<http://userwww.sfsu.edu/~ciotola/solar>
- Goetzberger, Adolf, Knobloch, Joachim, and Voss, Bernhard. Crystalline Silicon Solar Cells .England: John Wiley & Sons, 1998.
- Green, Martin A. Photovoltaics: Technology overview. *Energy Policy*, 28:989–998, 2000.
- Howes, Ruth and Fainberg, Anthony. T he Energy Sourcebook: A Guide to Technology,
http://energy.cr.usgs.gov/energy/stats_ctry/Stat1.html#PRODUCTION
<http://murray.newcastle.edu.au/users/students/2004/c2003616/intro.htm>
http://www.eere.energy.gov/RE/solar_photovoltaics.html
<http://www.jyotisha.00it.com/Latitude.htm#URUGUAY>
<http://www.rpc.com.au/products/panels/pvmodules/pvmodules.html>
<http://www.sandia.gov/pv/docs/PDF/IEDFB5~1.pdf>
<http://www.sandia.gov/pv/docs/PDF/kingkrat.pdf>
<http://www.sandia.gov/pv/docs/PDF/kingkrat.pdf>

http://www.solarelectricpower.org/power/pv_q&a.cfm#01

<http://www.wattsun.com/>

Johansson, Thomas B., Kelly, Henry., Reddy, Amulya K.N. and Williams, Robert H. eds. Renewable Energy: Sources for Fuels and Electricity Washington DC: Island Press, 1993.

Martin A. Green. *Solar cells*. Prentice-Hall, 1982

Montgomery, Douglas C., Design of Engineering Experiments, Wiley, 2005

Nansen, Ralph. Sun Power: The Global Solution for the Coming Energy Crisis. Ocean Press, Washington, 1995.

Partain, Larry D, ed. Solar Cells and Their Applications. New York: John Wiley & Sons, 1995.

Resources and Policy. American Institute of Physics, New York. 1991.

U.S. Geological Survey National Oil and Gas Resource Assessment Team, 1995, 1995

National Assessment of United States oil and gas resources: U.S. Geological Survey Circular 1118, 20 p.

Zweibel, Ken. Harnessing Solar Power: The Photovoltaics Challenge. New York: Plenum Press, 1990.

BIOGRAPHICAL SKETCH

Thomas P. Anthony was born in Bridgetown, Barbados in 1969. He is the first son and fifth child of George and Alexandrine Anthony. Thomas completed primary, secondary and tertiary technical education in Barbados. At the age of nineteen after a summer internship with Atlantis Submarines, a Canadian based company operating in Barbados, he was offered full time employment as a submarine copilot. This proved to be the catalyst that would lead him to an engineering education. After two years of intensive training, Thomas, at the age of twenty two was certified as the youngest submersible pilot in the world. Soon after certification, Thomas was chosen as a member of the international start-up crew to travel to Nassau, The Bahamas to start another company. It was during this time that he was promoted to submersible senior pilot and given the responsibility for the entire propulsion system of the submarine. This sparked a deep interest in the electrical engineering behind the systems with which he worked.

In 1998, Thomas applied and was accepted to Florida A&M University to study for a B.S. in electrical engineering. In August 2003, he graduated with honors with a concentration in power systems.

Thomas returned to Atlantis after graduation but after a short stint decided to pursue a graduate degree in industrial engineering. Florida State University was chosen for its reputation for research and attentive faculty. In December 2006, under the direction of his major professor Yaw A. Owusu, Thomas was awarded the Master's of Science degree in Industrial Engineering.